https://doi.org/10.5194/egusphere-2024-2866
Preprint. Discussion started: 30 September 2024

Intermodel comparison of the atmospheric composition changes due to emissions from a future supersonic aircraft fleet

Jurriaan A. van 't Hoff[1], Didier Hauglustaine[2], Johannes Pletzer[3], Agnieszka Skowron[4], Volker Grewe[1,3], Sigrun Matthes[3], Maximilian M. Meuser[3], Robin N. Thor[3], Irene C. Dedoussi[1,5]

[1]Aircraft Noise and Climate Effects Section, Faculty of Aerospace Engineering, Delft University of Technology, Delft, 2629 HS, The Netherlands

[2]Laboratoire des Sciences du Climat et de l'Environnement (LSCE), CEA-CNRS-UVSQ, Gif-sur-Yvette, 91190, France

[3]Deutsches Zentrum für Luft- und Raumfahrt, Institut für Physik der Atmosphäre, Oberpfaffenhofen, 82234 Weßling, Germany

[4]Faculty of Science and Engineering, Manchester Metropolitan University, Manchester, M1 5GD, United Kingdom

[5]Department of Engineering, University of Cambridge, Cambridge, CB3 0DY, United Kingdom

Correspondence to: icd23@cam.ac.uk

Abstract. Commercial supersonic aircraft may return in the near future, offering reduced travel times while flying higher in the atmosphere than present-day aircraft. Their emissions can change the composition of the atmosphere, particularly in the concentration and spatial distribution of ozone, aerosols, and greenhouse gases, posing risks to both the climate and public health. We present a comprehensive multi-model assessment of the impact of a supersonic fleet on a 2050 atmosphere using four state-of-the-art atmospheric models (EMAC, GEOS-Chem, LMDZ-INCA, MOZART-3). We show that the adoption of a fleet with a NO_x emissions index of 4.6 g(NO_2)/kg(fuel) leads to a model-mean stratospheric H_2O burden of +61.34 Tg for 46.2 Tg of annual H_2O emissions (model ranges from +20.14 to +116.53 Tg), and an ozone column loss of -0.11% (-0.18 to +0.03%). With a NO_x emissions index of 13.8 g(NO_2)/kg(fuel) the average ozone column loss increases to -0.31% (-0.57 to -0.09%). A lower cruise altitude and speed reduces the mean H_2O burden to +9.34 Tg (+2.37 to +19.69 Tg) and instead leads to an ozone column increase of +0.02% (-0.01 to +0.04%). Compared to the most recent multi-model assessment (2007), we find better agreement between the models, especially for the ozone response. Disagreement in H_2O perturbation lifetimes remains, potentially driven by differences in vertical model resolutions. Our results reaffirm that emissions from a supersonic aircraft fleet will lead to global changes in atmospheric composition, which can be reduced by adopting lower cruise altitudes and lowering NO_x emissions.

1 Introduction

Over the past decades there has been growing global demand for fast intercontinental transport. This demand has led to a search for faster alternatives to subsonic aircraft such as supersonic or even hypersonic transport vehicles (Kinnison et al. 2020, Pletzer et al. 2022). Supersonic vehicles have already attracted considerable commercial interest (Matthes et al. 2022, Eastham

https://doi.org/10.5194/egusphere-2024-2866
Preprint. Discussion started: 30 September 2024

et al. 2024). Several parties are currently working towards the reintroduction of supersonic civil transport aircraft, relying on new technologies such as low-boom hull designs meant to minimize the environmental impact of the sonic boom (Berton et al. 2020). An example of this development is NASA's X-59 demonstrator aircraft, which is planned to have its first flight this year.

Supersonic aircraft generally seek to use higher cruise altitudes to mitigate drag, with design cruise altitudes ranging from 14 to 21 km compared to subsonic altitudes which typically range between 9 and 12 km. The increase in operational altitude changes the atmospheric response to the so-called non-CO_2 emissions. Of particular concern is the interaction of nitrogen oxides (NO_x), water vapour (H_2O), and sulfur compound emissions with the ozone layer. The former two lead to catalytic destruction of ozone through the NO_x and HO_x cycles (Matthes et al. 2022, Grewe et al. 2007, Solomon 1999, Crutzen 1972, Johnston 1971), while the latter leads to the formation of sulfate aerosols (SO_4) which facilitate ozone destruction through heterogeneous chemistry (Pitari et al. 2014, Brasseur and Granier 1992). Combined with increased ozone formation from smog chemistry and the self-healing effect, this leads to changes in the distribution of stratospheric ozone and net column ozone depletion for high emission altitudes (Zhang et al. 2021a, Speth et al. 2021, Fritz et al. 2022, van 't Hoff et al., 2024a). This poses a risk to public health as the increased surface UV-exposure is linked to increased mortality (Eastham et al., 2018).

Besides an ozone impact, supersonic vehicles also have differing climate impacts compared to subsonic aviation. The climate impacts of supersonic vehicles are generally expected to be driven by H_2O emissions (Matthes et al. 2022, Pletzer et al. 2022, Zhang et al. 2021). Water vapour is a potent greenhouse gas which also plays an important role in the climate impact of subsonic aviation. At subsonic cruise altitudes (10 to 13 km) the perturbation lifetime of H_2O emissions is estimated to be between 1 and 6 months (Grewe and Stenke, 2008, Pletzer and Grewe, 2024). This limits its direct warming potential, but there is still considerable climate impact from the formation of contrails (Lee et al. 2021). At supersonic cruise altitudes (14 - 21 km) contrail formation is much less common as the stratosphere is drier (Stenke et al. 2008, Grewe et al. 2007, IPCC 1999). Instead, the perturbation lifetime of H_2O emissions is higher, up to around 1.5 years at 20 km (Grewe and Stenke, 2008). This leads to considerable accumulation of stratospheric H_2O, which is often found to be the main driver of the climate impact of emissions at these high altitudes (Grewe et al. 2010, Pletzer et al. 2022, Zhang et al. 2021a, Pletzer and Grewe 2024). Secondary to H_2O, the effect of changes in the global ozone distribution can have a warming effect, up to similar levels as those of H_2O emissions (Eastham et al. 2022).

Both the ozone and climate impacts stem from changes in the composition of the stratosphere. To adequately capture the changes in the chemical composition we rely on chemistry-transport models (CTMs) or chemistry-climate models (CCMs), which model the chemistry, transport, removal, and conversion of species throughout the atmosphere. A variety of such models has already been used to evaluate the effects of high-altitude emissions on ozone and the climate, and despite their similar scope and chemistry routines this often leads to different results in the impact assessments for the future adoption of supersonic

https://doi.org/10.5194/egusphere-2024-2866
Preprint. Discussion started: 30 September 2024

aircraft. These differences are in part driven by uncertainties about the future of supersonic civil aviation, resulting in the use of different emission scenarios and timelines across studies. However, earlier multi-model studies also highlight that there are considerable differences between the CTMs and CCMs even in the evaluation of identical scenarios (e.g. Grewe et al., 2007; Kawa et al. 1999, Pitari et al. 2008), thereby making previous results dependent on model choice. These differences are most prevalent in the evaluation of changes in ozone, the impact on which is subject to complex feedback mechanisms. In earlier multi-model studies the ozone impact predictions sometimes conflict, with models predicting net column increases and decreases (Kawa et al. 1996) or if they agree on depletion there is still a large spread (Grewe et al. 2007). These differences are also observed through comparison of ozone sensitivities to emissions between models (Eastham et al. 2022, van 't Hoff et al. 2024a). They are often driven by different implementations of key chemical, transport, or radiative processes across the models, especially the interactions between these components, while also being affected by other properties such as model resolutions.

Understanding the effect of model-driven differences in the evaluation of high-altitude emission impacts is vital to our capability to synthesize results across studies that use different models. Multi-model studies expose these differences and can help us understand their drivers, potentially offering robust conclusions and policy advice. In the field of high-altitude emissions, the most recent multi-model study performed by Grewe et al. (2007) showed that while all models agreed on the introduction of supersonic emissions leading to net depletion of ozone and increases in radiative forcing, there were still considerable differences between the models' estimates of changes in ozone distribution and the stratospheric H_2O accumulation. They report a multi-model mean depletion of 8 Tg with a standard deviation of 5.49 Tg, and for H_2O a mean perturbation of 64 Tg with a standard deviation of 20.03 Tg. These differences are not to be underestimated, but also indicate a notable improvement over models used by Kawa et al. (1999) who, with 7 models, found a mean column ozone depletion of -0.16% with a standard deviation of 0.17% for a similar supersonic emission scenario. Since then, there have been considerable advances in our understanding of the underlying chemistry and physics, and at the same time rapid increases in computational power have expanded our capacity to model these processes. This has led to enhancements in the overall modelling capabilities of CTMs. To assess the effect of these developments Zhang et al. (2021a) have recently compared the modern WACCM6 model to models used by Kawa et al. (1999) in a reassessment of their scenarios, finding similar overall atmospheric impacts despite the higher detail in their model. While this does provide some insight with respect to older evaluations, it remains unclear whether the past two decades of model development have led to better convergence in the assessment of supersonic emissions in currently widely used models.

To close this gap, we re-evaluate existing supersonic emission scenarios from the most recent multi-model study on the SCENIC project (Grewe et al., 2007). We do this with four state-of-the-science atmospheric chemistry-climate and chemistry-transport models (EMAC, GEOS-Chem, LMDZ-INCA, MOZART-3), comparing the atmospheric changes induced by different supersonic emissions within these models with the earlier results and we analyse differences in atmospheric

https://doi.org/10.5194/egusphere-2024-2866
Preprint. Discussion started: 30 September 2024

responses, emphasizing the effects of H_2O, NO_x, and O_3 perturbations as simulated by the different models. We present the output of these models in a harmonized way, in order to provide a comprehensive, multi-model estimate of the impacts of supersonic aircraft emissions in the stratosphere.

2 Methodology

2.1 Emission scenarios

We study the impact of supersonic aircraft emission scenarios derived from the SCENIC project (Grewe et al., 2007) in a 2050 atmosphere based on the CMIP6 SSP3.7 scenario (Riahi et al. 2017). The SCENIC emission inventories consider the adoption of a fleet of 501 supersonic transport aircraft for the partial replacement (around 4% of revenue passenger km) of subsonic aviation. The supersonic aircraft operate at a cruise speed of Mach 2 at cruise altitudes from 16.5 to 19.5 km (Grewe et al. 2007, Grewe and Stenke 2008). We use the same global distribution of supersonic flight routes, accounting for the partial substitution of subsonic traffic with the supersonic counterparts (Grewe and Stenke 2008). This leads to reduction in global fuel consumption of around 3.3% when compared to the emissions of the Grewe et al. (2007) study. The characteristics of the emission scenarios are summarized in Table 1.

Table 1: Summary of the aircraft emission scenarios. The baseline emission scenario (A0) has no supersonic aviation. The nominal supersonic emissions scenario (A1) considers the partial replacement of subsonic traffic with supersonic vehicles. Of this scenario two variants are included with triple supersonic NO_x emissions (A2) and a lower cruise supersonic altitude and speed (A3). The left columns summarize the emission characteristics of all combined aircraft (subsonic and supersonic), and the right columns summarize the supersonic aircraft emissions.

	All Aircraft			Supersonic aircraft			
	Annual fuel consumption (Tg a^{-1})	Annual NO_x emissions ($Tg(NO_2)$ a^{-1})	Average EI NO_x (g NO_2 / kg)	Annual fuel consumption (Tg a^{-1})	Annual NO_x emissions ($Tg(NO_2)$ a^{-1})	Average EI NO_x (g NO_2/kg)	Cruise altitude [km]
A0 (Baseline)	656.40	7.16	10.91	-	-	-	-
A1 (Nominal)	697.87	7.23	10.36	57.93	0.27	4.60	16.5-19.5
A2 (Triple NO_x)	697.87	7.75	11.11	57.93	0.80	13.80	16.5-19.5
A3 (Low cruise)	679.04	7.20	10.33	40	0.22	5.62	13.1-16.7

We consider a baseline scenario (A0) with only subsonic aviation emissions (S0 from Grewe et al. 2007). The nominal supersonic scenario (A1) considers the partial replacement (4.1 % of passenger km) of subsonic aviation with a supersonic

https://doi.org/10.5194/egusphere-2024-2866
Preprint. Discussion started: 30 September 2024

transport fleet (S5 of Grewe et al. 2007). This substitution results in an increase of 6.3% in global aviation fuel usage. The triple NO_x scenario (A2) is a variant of the nominal scenario with tripled supersonic NO_x emissions, resulting in a fleet-average supersonic emission index of 13.80 kg NO_2/kg which is closer to supersonic NO_x emission estimates from more recent studies (Speth et al. 2021; Zhang et al. 2021a; Fritz et al. 2022). Finally, in the low cruise scenario we consider the use of a different aircraft concept with a lower cruise altitude of 13.1 to 16.7 km and a cruise speed of Mach 1.6 (P6 from Grewe et al. 2007). Compared to the nominal emissions this leads to a 5.5% reduction in supersonic passenger kilometres and a 31% reduction in supersonic fuel consumption. The resulting changes in the distribution of aviation emissions is shown in Fig. 1.

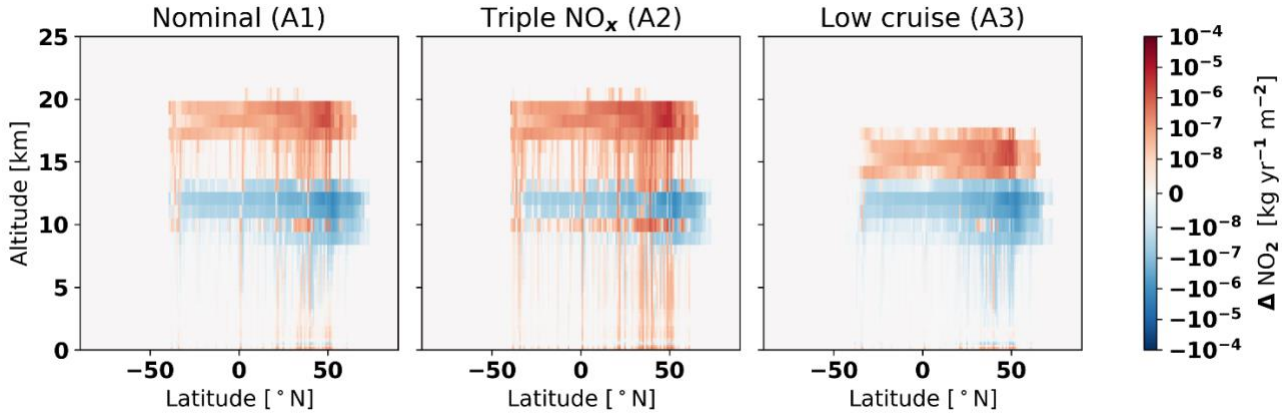

Fig 1: Zonal mean changes in the vertical distribution of annual NO_x emissions (expressed in kg NO_2) due to the introduction of supersonic aviation. Differences are calculated with respect to the annual A0 emissions.

2.2 Atmospheric modelling

Numerical simulations are performed using four widely used global chemistry transport models: EMAC, GEOS-Chem, LMDZ-INCA, MOZART-3. A summary of the characteristics of the models, including resolution, chemistry processes covered, and dynamics is provided in Table 2 and the individual models are detailed in the following subsections.

Table 2: Summary of the atmospheric models characteristics, including resolution, chemistry, and dynamics

Model	Resolution (lat × lon)	Vertical domain & resolution	Chemistry	Dynamics	Reference
EMAC	T42 (~2.8°×2.8°)	Surface to 0.01 hPa, 90 hybrid levels	1202 species 1839 gas phase rcts. 401 aqueous rcts. 401 photolytic rcts. 27 aqueous phase photolytic rcts. 21 heterogeneous rcts.	ECHAM5 nudged to ERA5	Jöckel et al. 2016 Roeckner et al. 2003 Sander et al. 2011

https://doi.org/10.5194/egusphere-2024-2866
Preprint. Discussion started: 30 September 2024

GEOS-Chem	C48 (~2°×2.5°)	Surface to 0.01 hPa, 72 hybrid levels.	132 species 344 kinetic rcts. 154 photolytic rcts. 78 heterogeneous rcts.	MERRA -2, no online meteorology	Eastham et al. 2018 Eastham et al. 2014
LMDZ-INCA	1.3°×2.5°	Surface to 0.04 hPa, 39 hybrid levels	154 species 234 homogeneous rcts. 43 photolytic rcts. 30 heterogeneous rcts.	LMDZ nudged to ERA5	Hauglustaine et al. 2014. Terrenoire et al. 2022.
MOZART-3	T42 (~2.8°×2.8°)	Surface to 0.1 hPa, 60 hybrid layers	108 species 218 gas phase rcts. 71 photolytic rcts. 18 heterogeneous rcts.	ERA-Interim, no online meteorology	Kinnison et al., 2007 Skowron et al., 2021

2.2.1 EMAC

EMAC is an atmospheric chemistry general circulation model, consisting of the dynamical core ECHAM5 (European Centre HAMburg general circulation model, version 5, Roeckner et al. 2006) and MESSy (Modular Earth Submodel System, Jöckel et al. 2016). We use version 2.55.2 (The MESSY Consortium, 2021) of the EMAC model with a T42 global grid (approximately 2.8° × 2.8° latitude, longitude) and 90 hybrid vertical levels from the surface up to 80 km. The chemical mechanism incorporates 1839 gas phase and 21 heterogeneous phase reactions between 1202 species, which includes type 1ab and type 2 polar stratospheric clouds (PSC, Kirner et al. 2010; Jöckel et al. 2010). The reaction rates are from the most recent Jet Propulsion Laboratory evaluation number 19 (Burkhold et al. 2020). Aerosol background concentrations are provided for heterogeneous chemistry.

The model is nudged towards ERA5 reanalysis data (2000-2010) between the surface and 10 hPa. Nudging is applied in the same way as earlier studies (Jöckel et al. 2016; Pletzer et al. 2022), affecting horizontal and vertical winds, temperature (wave 0 omitted), and the logarithm of surface pressure. Water vapour is accounted for as specific humidity q, which is influenced by gas-, solid- and liquid-phase processes at all altitudes. It is produced through 55 reactions and destroyed through six reactions, and it is affected by physical processes such as rain-out and sedimentation. The radiation scheme incorporates 81 bands and recreates the solar cycle with high fidelity. This applies to the region from the top of the model domain (0.01 hPa) to 70 hPa (Kunze et al. 2014; Dietmüller et al. 2016). Background atmosphere and non-aviation anthropogenic emissions are based on the CMIP6 SSP3 7.0 scenario for the year 2050.

For EMAC model simulations a spin up method was applied, which allows to reduce spin up times while maintaining annual quasi-equilibrium. During the first year of simulations the annual aircraft emissions are increased by an altitude-dependent scaling factor, and standard values are applied after. Through this approach annual quasi-equilibrium is achieved faster. For

https://doi.org/10.5194/egusphere-2024-2866
Preprint. Discussion started: 30 September 2024

more detail on this method, we refer to the work by Pletzer and Grewe (2024) and its supplement. The model is integrated for a total of 16 years to allow for a longer averaging period, which is done to improve the statistical significance of the EMAC results.

2.2.2 GEOS-Chem

GEOS-Chem is a community-developed tropospheric-stratospheric CTM with over 280 chemical species based on the Goddard Earth Observing System (GEOS) (Bey et al. 2001). It incorporates stratospheric chemistry through the Unified Tropospheric-Stratospheric Chemistry Extension (UCX) by Eastham et al. (2014) using KPP for kinetic chemistry (Damian et al. 2002) and Fast-JX for photolytic reactions (Bian and Prather, 2002). Within the troposphere H_2O mixing ratios are prescribed by the offline meteorology, and in the stratosphere the H_2O tracer evolves freely subject to photochemical chemistry and tropospheric-stratospheric transport. GEOS-Chem's capability to model stratospheric chemistry extension has been demonstrated against satellite observations across several studies (Eastham et al. 2014; Speth et al. 2021; Fritz et al. 2022; van 't Hoff et al. 2024a), and it is incorporated into NASA GMAO's GEOS chemical composition forecast (GEOS-CF) (Keller et al. 2021).

We use version 14.1.1 of the GEOS-Chem High Performance variant (The International GEOS-Chem User Community, 2023) with a C48 cuboid-spherical global grid (approximately 2° × 2.5° latitude, longitude) and 72 non-uniform vertical levels. We use historical meteorological data for the years 2000 to 2010 from the MERRA-2 reanalysis product by NASA/GMAO (Gelaro et al. 2017). Volcanic emissions are incorporated through historical emissions for the same time period following work by Carn et al. (2015). The model simulations are run for a total of 10 years using the spin up method as EMAC, detailed in Pletzer and Grewe (2024).

2.2.3 LMDZ-INCA

The LMDZ-INCA global chemistry-aerosol-climate model couples online the LMDZ (Laboratoire de Météorologie Dynamique, version 6) General Circulation Model (Hourdin et al., 2020) and the INCA (INteraction with Chemistry and Aerosols, version 6) model (Hauglustaine et al., 2004; 2014). In the present configuration, we use the "Standard Physics" parameterization of the GCM (Boucher et al., 2020). The model includes 39 hybrid vertical levels extending up to 70 km. The horizontal resolution is 1.3° × 2.5° in latitude and longitude, respectively. The primitive equations in the GCM are solved with a 3 min time-step, large-scale transport of tracers is carried out every 15 min, and physical and chemical processes are calculated at a 30 min time interval. The large-scale advection of tracers is calculated based on a monotonic finite-volume second-order scheme (Van Leer, 1977; Hourdin and Armengaud 1999). Deep convection is parameterized according to the scheme of Emanuel (1991). The turbulent mixing in the planetary boundary layer is based on a local second-order closure formalism.

https://doi.org/10.5194/egusphere-2024-2866
Preprint. Discussion started: 30 September 2024

INCA includes a state-of-the-art CH_4-NO_x-CO-NMHC-O_3 tropospheric photochemistry (Hauglustaine et al., 2004; Folberth et al., 2006). For aerosols, the INCA model simulates the distribution of aerosols with anthropogenic sources such as sulfates, nitrates, black carbon (BC), organic carbon (OC), as well as natural aerosols such as sea-salt and dust. The heterogeneous reactions on both natural and anthropogenic tropospheric aerosols are included in the model (Hauglustaine et al., 2004; 2014). This version of the model also includes an interactive chemistry in the stratosphere and mesosphere (Terrenoire et al., 2022). Heterogeneous processes on PSCs and stratospheric aerosols are parameterized following the scheme implemented in Lefèvre et al. (1994). Water vapour is affected by physical processes in the LMDZ GCM and an additional H_2O tracer is introduced in INCA in order to account for photochemical production and destruction. Below the model tropopause, the two water vapour tracers (i.e., physical water vapour tracer and full water vapour tracer) are imposed identical at each time-step, and only the full H_2O tracer is affected by chemistry (and aircraft emissions) in the stratosphere. In addition to gas phase chemistry, in the stratosphere, condensation and further sedimentation of water vapour can occur over stratospheric aerosols and PSCs at high (>60°) latitudes. The model simulations have a 15 year duration with initial conditions representative of the year 2050 (Pletzer et al., 2022) and with surface emissions provided by the CMIP6 SSP3-7.0 scenario. In this study, the LMDZ GCM zonal and meridional wind components are nudged towards the meteorological data from the European Centre for Medium-Range Weather Forecasts (ECMWF) ERA-Interim reanalysis, with a relaxation time of 3.6 h (Hauglustaine et al., 2004). The ECMWF fields are provided every 6 h and interpolated onto the GCM grid for the years 2004-2018.

2.2.4 MOZART-3

The Model for OZone And Related chemical Tracers, version 3 (MOZART-3) is an offline chemical transport model (Kinnison et al., 2007) which has been used for an extensive range of applications (e.g., Liu et al., 2009; Flemming et al., 2011including various aspects of the impact of aircraft NO_x emissions on atmospheric composition (e.g., Sovde et al., 2014; Skowron et al., 2013, 2015, 2021, Freeman et al., 2018). MOZART-3 accounts for advection based on a flux-form semi-Lagrangian scheme, a shallow and mid-level convective and deep convective routines, boundary layer exchanges, and wet and dry deposition. MOZART-3 reproduces detailed chemical and physical processes from the troposphere through the stratosphere, including gas-phase, photolytic and heterogeneous reactions. The kinetic and photochemical data are based on the NASA/JPL evaluation (Sander et al., 2006). The H_2O emissions have been implemented into the model for the purpose of this work allowing H_2O to evolve freely in the stratosphere and fixing it in the troposphere. However, it is still under exploration due to probable limitations with tropospheric-stratospheric transport.

In this work we use a model configuration with a T42 (~ 2.8° × 2.8°) horizontal resolution and 60 hybrid layers from the surface to 0.1 hPa. The transport of chemical compounds is driven by the meteorological fields from the European Centre for Medium Range Weather Forecast (ECMWF), 6 h reanalysis ERA-Interim data for the year 2006. The 2050 gridded surface emissions (anthropogenic and biomass burning) were determined by Integrated Assessment Models (IAMs) for the business-as-usual scenario of the Representative Concentration Pathways, RCP 4.5. The model was run for 8 years until reaching a

https://doi.org/10.5194/egusphere-2024-2866
Preprint. Discussion started: 30 September 2024

steady-state and the last year of these simulations is considered for the analysis. For the assessment of the H_2O separate model runs were used with outputs in limited vertical resolution of 30 layers from 200 to 0.1 hPa.

2.2.5 Atmospheric conditions

We evaluate the impact of the supersonic aircraft emission scenarios in a 2050 atmosphere, which is an appropriate timeframe for large-scale civil application of these aircraft and matches the adoption timeframe considered by Grewe et al. (2007). Due to differences in the availability of datasets across all models, we make some compromises in the model setup to ensure better compatibility across the simulation setups. Notably we use historical data (2000-2020) for the inputs of background meteorology and volcanic emissions rather than future forecasts. In the EMAC, GEOS-Chem, and LMDZ-INCA models we base the atmosphere and surface emissions on the SSP 3.7 socioeconomic pathway from CMIP 6 (Riahi et al. 2017). This is different for the MOZART-3 model, where this is based on RCP 4.5 instead and the model is driven by more constrained meteorology (yearly data for 2006). Compared to the other models this means we expect less availability of methane (CH_4) and nitrogen compounds in MOZART-3's atmosphere (Meinshausen et al. 2020).

3 Results & Discussion

With this work we present a comprehensive review of the effects of supersonic aviation on the atmospheric composition as observed by several state-of-the-art models for the first time since the work by Grewe et al. (2007). Firstly, we will give a summary of the impact of the supersonic emissions on the stratospheric composition in section 3.1. These impacts are calculated over the last three years of the model integrations for GEOS-Chem and LMDZ-INCA. For the EMAC results we use 6 years to improve the statistical significance, and the MOZART-3 results show an annual average due to its cycling meteorology. The individual impacts on stratospheric water vapour, NO_x and NO_y, ozone, and odd oxygen loss rates are then discussed in more detail in sections 3.2 to 3.5. In these sections we also explore the differences between the individual models.

3.1 Global atmospheric impact

Table 3 provides a summary of the key variables representing the changes in atmospheric composition in response to the emissions across all models. Similar to Grewe et al. (2007), we include the hemispheric fraction, which is the ratio of the perturbation mass in the northern hemisphere over the perturbation mass in the southern hemisphere, as a means to quantify interhemispheric transport. For the nominal supersonic scenario (A1) we find stratospheric H_2O perturbations ranging between 20.55 Tg (+0.55%) for the LMDZ-INCA model to +116.53 (+1.55%) for MOZART-3, with a multi-model mean perturbation of 61.34 Tg and a mean perturbation lifetime of 16.7 months. The mean perturbation lifetime (e-folding lifetime) is calculated by dividing the stratospheric perturbation by the increase in annual stratospheric emissions. This perturbation is largely retained in the northern hemisphere, as indicated by the mean hemispheric fraction of 4.68. There is good agreement in the stratospheric NO_x perturbation across the models, ranging from +38.71 Tg for EMAC to +43.52 for GEOS-Chem with a model-mean of

https://doi.org/10.5194/egusphere-2024-2866
Preprint. Discussion started: 30 September 2024

+40.96 Tg. The emissions cause in a mean change of global column ozone by -0.11 %, with a range of -0.22 % for GEOS-Chem to +0.03% for EMAC.

These results are similar to the results of Grewe et al. (2007), who report a model-mean H_2O perturbation of 64 Tg with a range of 45 to 98 Tg between models. Compared to their work we do note an increase in the overall hemispheric fraction. Grewe et al. report a model-mean value of 2.96 which is smaller than our mean, indicating reduced hemispheric exchange in our models. The source of this will be discussed further in section 3.2. Grewe et al. (2007) also report a mean change in the overall ozone column of -8 Tg, with a spread of -1 to -16 Tg between their models. Here we note a considerable improvement in the agreement of the ozone response in the models, as we find a smaller spread in the ozone perturbation mass and hemispheric fraction (Fig. A1).

In the triple NO_x emission scenario (A2) the tripling of the NO_x emissions index increases the stratospheric NO_x accumulation by a factor of 3.4. There is little change in terms of the H_2O perturbation, but ozone depletion increases to a mean ozone column change of -0.31 %, ranging between -0.57% for MOZART-3 to -0.09% for LMDZ-INCA. We note that the NO_x response is non-linear across all models. The tripling of supersonic NO_x emissions increases stratospheric O_3 loss by factors of 2.39 and 2.56 for the GEOS-Chem and LMDZ-INCA models, whereas this factor is 3.89 for MOZART-3 and 7.24 for EMAC (Table A3). The higher sensitivity of MOZART-3 may be driven by its lower background nitrogen availability (Table A2), whereas that of EMAC is enhanced by the low stratospheric O_3 loss for the nominal scenario. Still, the high factor for EMAC in particular may also be indicative of strong non-linear interactions. These drivers are expanded on in subsequent sections.

The impacts on stratospheric composition are reduced for the low cruise altitude scenario (A3). Here we find a mean H_2O perturbation of +9.34 Tg with a mean lifetime of 5.3 months. In this case very little H_2O reaches the southern hemisphere, resulting in high hemispheric fractions, with values of -25.07, 10.19, and 36.26 respectively for EMAC, GEOS-Chem, and LMDZ-INCA. The negative value for EMAC is due to a net-decrease in southern hemispheric H_2O. The reduction in cruise altitude also reduces the NO_x perturbation to a mean +20.82 Tg, ranging from +17.41 to +23.72 Tg. In this low cruise scenario we find a mean increase of the overall ozone column across the models with the exception of GEOS-Chem, which calculates a -0.01% change. This results in a model-mean ozone increase of +0.02% with a range of -0.01% to +0.04%.

https://doi.org/10.5194/egusphere-2024-2866
Preprint. Discussion started: 30 September 2024

Table 3: Summary of impacts on stratospheric water vapour budget and ozone column changes for the emission scenarios. These impacts are calculated as differences between the scenarios and the baseline. For more extensive summaries of the H_2O, NO_x, and O_3 impacts including background mass budgets see Tables A1 to A3 in the appendix. *The H_2O perturbation lifetime of the MOZART-3 model may be excessive due to some limitations in the H_2O evaluation, see the discussion at the end of section 3.2.

	H_2O perturbation [Tg] (relative [%])	H_2O hemispheric fraction [NH/SH]	H_2O perturbation lifetime [months]	NO_x perturbation [Tg NO_2] (relative [%])	NO_x perturbation lifetime [months]	Ozone column change [DU] (relative [%])
Nominal (A1)						
EMAC	+69.34 (+1.62 %)	4.82	17.8	+38.71 (+1.67%)	4.2	+0.09 (+0.03 %)
GEOS-Chem	+49.34 (+0.67%)	3.96	12.7	+43.52 (+1.89%)	4.7	-0.72 (-0.22 %)
LMDZ-INCA	+20.14 (+0.58%)	5.37	5.2	+42.56 (+1.73%)	4.6	-0.15 (-0.05 %)
MOZART-3	+116.53* (+ 1.55 %)	4.56	30.0*	+39.07 (+3.16 %)	4.2	-0.43 (-0.18%)
Mean	+61.34 (+1.11 %)	4.68	16.4	+40.96 (+2.11 %)	4.4	-0.30 (-0.11 %)
Triple NO_x (A2)						
EMAC	+66.27 (+1.54 %)	7.05	17.0	+139.6 (+6.01 %)	3.3	-0.611 (-0.18 %)
GEOS-Chem	+49.79 (+0.68 %)	3.88	12.8	+173.6 (+7.54 %)	4.1	-1.36 (-0.41%)
LMDZ-INCA	+20.55 (+0.55 %)	5.11	5.3	+119.54 (+4.86 %)	2.8	-0.30 (-0.09 %)
MOZART-3	-	-	-	+120.74 (+9.79 %)	2.8	-1.35 (-0.57 %)
Mean	+45.54 (+0.92 %)	5.35	7.48	+138.37 (+7.05 %)	3.3	-0.91 (-0.31 %)
Lower cruise (A3)						
EMAC	+19.69 (+0.46 %)	-25.07	11.2	+21.32 (+0.92 %)	5.4	+0.11 (+0.03 %)
GEOS-Chem	+5.96 (+0.08 %)	10.19	3.4	+23.72 (+1.03 %)	6.0	-0.04 (-0.01 %)
LMDZ-INCA	+2.37 (+0.06%)	36.26	1.3	+17.41 (+0.71 %)	4.4	+0.14 (+0.04 %)
Mean	+9.34 (+0.20 %)	8.89	5.3	+20.82 (+0.89 %)	5.3	+0.07 (+0.02 %)

https://doi.org/10.5194/egusphere-2024-2866
Preprint. Discussion started: 30 September 2024

3.2 Water vapour

Figure 2 shows the H_2O perturbations from the nominal supersonic scenario (A1) as evaluated across the four models, the vertical averages are shown in Fig. 3. Overall, the perturbation patterns of stratospheric water vapour in the zonal mean distributions agree across the models. The strongest changes in stratospheric H_2O concentrations occur around the cruise altitude in the northern hemisphere, coinciding with the majority of supersonic activity. From the cruise areas we see extensions transporting H_2O to the northern polar latitudes, and upwards transport to the upper stratosphere in tropical latitudes. Similar accumulation patterns have been observed across other studies (Zhang et al. 2023;2021a;2021b, Kinnison et al. 2020). Our results are similar to results from Grewe et al. (2007) up to pressure altitudes of 60 hPa. Above this altitude our model results show stronger perturbations, which may be related to the extended vertical domain.

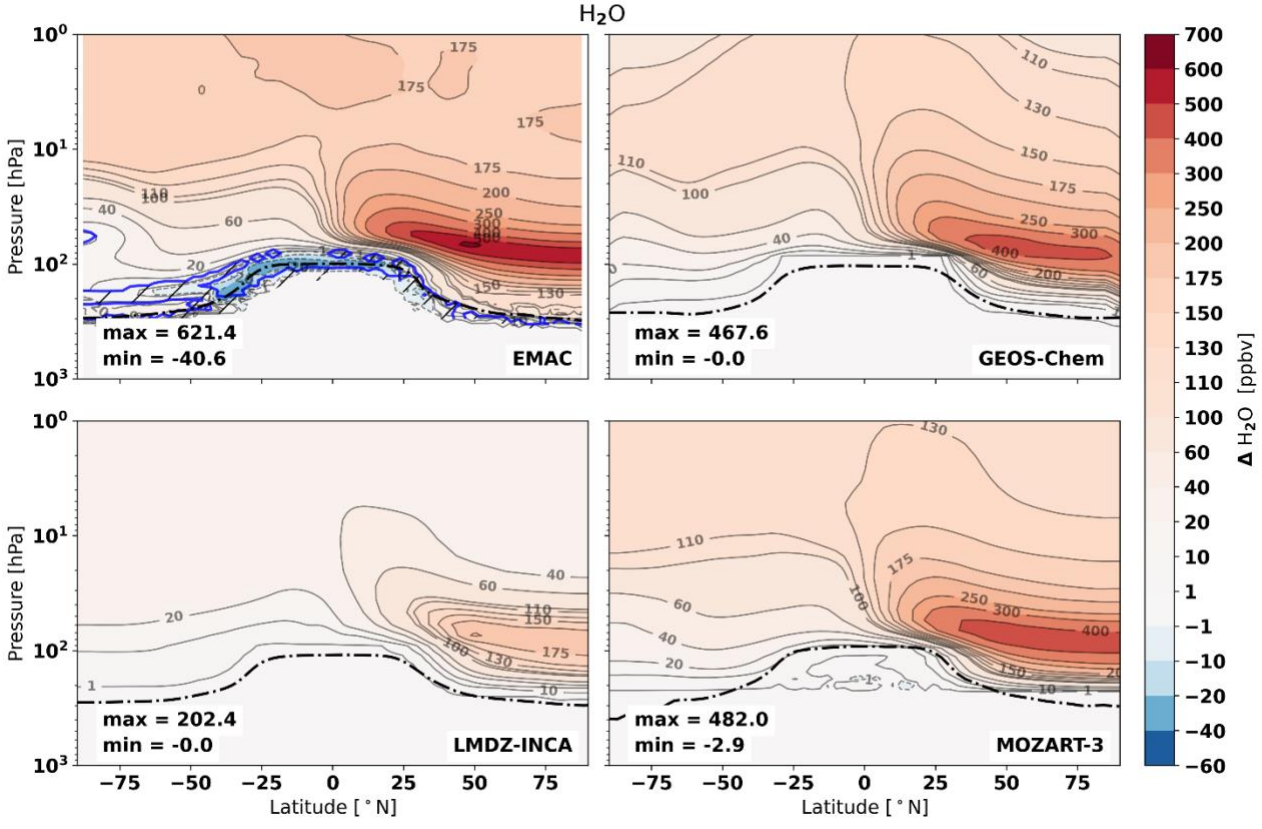

Fig 2: Mean changes in H_2O mixing ratios (ppbv) in response to the supersonic emissions scenario (A0). Hatched areas enclosed by blue lines indicate regions which are not statistically significant for the EMAC results. Similar figures for the triple NO_x and low cruise scenarios are provided in the appendix (Fig A2, A3).

https://doi.org/10.5194/egusphere-2024-2866
Preprint. Discussion started: 30 September 2024

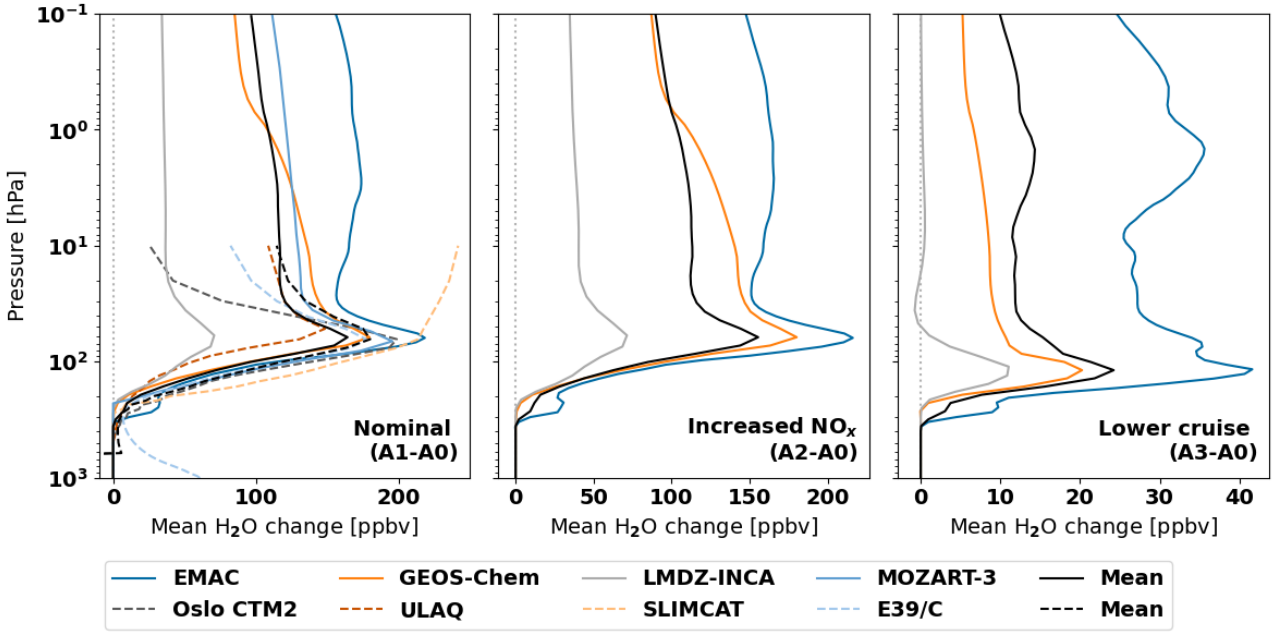

Fig 3: Mean changes in H_2O mixing ratio over altitude for the nominal supersonic (A1, left), triple NO_x (A2. middle) and low cruise (A3, right) emission scenarios. Entries with dashed lines are from data from Grewe et al. 2007.

As previously mentioned, we find larger hemispheric fractions in our results compared to those of Grewe et al. (2007), indicating a reduced interhemispheric exchange in our models. Their hemispheric fractions range from 1.8 to 4.2 with a mean of 2.96, whereas ours range between 3.96 to 5.37 with a model-mean of 4.68. We expect that this difference is driven by an improved representation of the tropical pipe acting as a transport barrier through a finer horizontal resolution in our models. Previous work has shown that the horizontal resolution is important in the representation of horizontal mixing and diffusion, and that coarse resolutions can lead to over-estimations of horizontal mixing (Strahan and Polansky, 2006). Consequently, we note a trend between the horizontal model resolution and the hemispheric fraction, leading to reduced interhemispheric exchange with finer horizontal resolutions (Fig. A4).

Between the models we find notable discrepancies in the stratospheric H_2O perturbation lifetime. Here we will first discuss the difference between the EMAC, GEOS-Chem, and LMDZ-INCA models which model H_2O over the full tropo- and stratosphere. This is not the case for MOZART-3, which is discussed separately afterwards. Between the EMAC, GEOS-Chem, and LMDZ-INCA models we hypothesize that the discrepancy in H_2O perturbation lifetimes may be driven by differences in the model treatment of tropospheric H_2O and the models' vertical resolutions. In the GEOS-Chem and LMDZ-INCA models tropospheric H_2O is fixed to the model meteorology. In this case the model troposphere acts as a sink for stratospheric H_2O tracers as the perturbation is removed when transported into the upper troposphere. As the tropopause height in high latitudes is adjusted seasonally, parts of the model grid switch from stratospheric to tropospheric, stripping the stratospheric H_2O near the boundary. This may lead to excessive removal of lower-stratospheric H_2O, particularly at high

https://doi.org/10.5194/egusphere-2024-2866
Preprint. Discussion started: 30 September 2024

latitudes, which is also enhanced by lower vertical resolution around the UTLS interface. This stripping effect has been observed to reduce H_2O perturbation lifetimes in the GEOS-Chem model (van 't Hoff et al., 2024a) and we expect it may play a role here as well. In addition, similar to the effect of horizontal resolutions on horizontal transport modelling, the vertical resolution is also critical to the modelling of vertical transport and diffusion processes (Revell et al. 2015, Roeckner et al. 2006). Revell et al. (2015) have shown that the 90 layer EMAC model has reduced tropical upwards mass flux compared to the 47 layer model, and Brinkop et al. (in preparation, personal correspondence) also report that 90 layer EMAC simulations more accurately recreate stratosphere-troposphere exchange patterns than the 47 layer counterpart.

This is reflected by the identification of a clear trend between the vertical model resolution and the H_2O perturbation lifetime between the EMAC, GEOS-Chem, and LMDZ-INCA results. The LMDZ-INCA model, which has the coarsest vertical resolution at 39 levels, also has the lowest H_2O perturbation lifetimes. EMAC with 90 layers has the highest perturbation lifetimes, and GEOS-Chem's resolution and lifetime fit well to a linear trend in-between (Fig. A5). We also note that the shorter perturbation lifetime in LMDZ-INCA may be enhanced by overestimations of cross-tropopause transport at high latitudes (Cohen et al. 2023). The effect of the H_2O sink and vertical resolution is greatly enhanced for emissions in close proximity to the tropopause, and it reduces for high-altitude emissions. This explains why we find larger discrepancies for the low cruise (A3) emissions scenario. In this case we find a mean lifetime of 5.3 months, ranging from 1.3 months for LMDZ-INCA to 11.2 months for EMAC. Compared to the nominal supersonic scenario (A1) the perturbation lifetime is reduced by 37% for EMAC, for the GEOS-Chem and LMDZ-INCA models the respective lifetimes and decreases are 3.4 (-73%) and 1.3 (-75%) months. We also link this relationship to results from Pletzer et al. (2022) who used similar setups in the EMAC and LMDZ-INCA models in tandem to study the impact of even higher altitude (26 to 35 km) emissions. In their results they also find LMDZ-INCA has lower H_2O perturbation lifetimes compared to EMAC, with a relative difference of -8.6% at for 35 km emissions to -20.3% at 26 km cruise altitudes (Pletzer et al. 2022). Between these models we find a relative difference of -70.8% and -88.4% at mean cruise altitudes 18 and 14.9 km respectively, fitting the expected increase in stratospheric H_2O perturbation loss with lower emission altitudes.

In this consideration we have not included the MOZART-3 model, which has considerably higher perturbation lifetimes, as it is subject to some fundamental differences from the other models. Contrary to the other models which have H_2O as internal tracers, MOZART-3's perturbation is calculated through a separate model run with a different vertical grid. Like the GEOS-Chem and LMDZ-INCA models this also uses fixed tropospheric H_2O mixing ratios, but the vertical grid does not extend past 200 hPa. Because of this limit it does not capture interactions of stratospheric H_2O with the tropopause outside of lower latitudes where there is predominantly upwards vertical transport, and as a result it may be missing crucial sinks of stratospheric H_2O at high latitudes. Furthermore, the separation of H_2O tracers from the CTM may mean that H_2O sinks from chemistry are not fully incorporated, or they could be weaker than in integrated models. Combined this results in the high H_2O perturbation lifetime in MOZART-3, which does not fit the other models.

https://doi.org/10.5194/egusphere-2024-2866
Preprint. Discussion started: 30 September 2024

3.3 Odd and reactive nitrogen

Figure 4 shows the perturbation of reactive nitrogen (NO_x) and odd nitrogen (NO_y) from the nominal supersonic emissions (A1) over the four models. Similar figures for the triple NO_x and low cruise scenarios are provided in the appendix. We define NO_y as $NO_y = NO + NO_2 + NO_3 + HNO_2 + HNO_3 + HNO_4 + ClNO_3 + 2\ N_2O_5 + PAN + ClNO_2 + BrNO3$. In these perturbations we observe similarities across all models. The NO_x responses are primarily concentrated around the equator, with the strongest accumulation in the middle-stratosphere and a secondary zone near the northern equatorial tropopause. In contrast to the NO_x perturbation, the accumulation of NO_y is concentrated around the cruise emission area in all models. This perturbation, which includes that of NO_x, is mostly driven by strong formation of HNO_3 in these areas. The odd nitrogen is then transported to the north pole or southwards to the tropical pipes, where it makes its way to the middle stratosphere. This results in similar accumulation patterns for NO_y as is observed for H_2O emissions. Similar NO_y perturbations from supersonic aviation have been observed by Zhang et al. (2023,2021a) and by Kinnison et al. (2020) with the WACCM model.

The NO_x and NO_y perturbations are similar across all models except for EMAC, where we find substantial differences in the upper stratosphere and southern hemisphere. Contrary to the other models EMAC predicts a loss of NO_x and NO_y in these areas, and the same can be observed for the triple NO_x and low cruise scenarios (Fig A6, A7). The differences are particularly striking above a pressure altitude of 10 hPa, where EMAC's meteorology is not nudged. This leads to a deviation of meteorological parameters between the base run and the perturbed run, due to a combined result of the butterfly effect (noise) and meteorological feedbacks from the changes in stratospheric composition (Deckert et al. 2011). Because of this, parts of EMAC's upper atmospheric response are not statistically significant with the current model integration time. Still, we do find areas NO_x and NO_y depletion which are significant in the upper-stratosphere, suggesting that we do also see the effect of feedback mechanisms,

Comparing the model temperatures we find that the introduction of the supersonic emissions leads to overall cooling of EMAC's stratosphere (Fig A8). Near the south pole between 100 and 10 hPa this cooling is approximately 0.15 K, facilitating increased formation of polar stratospheric clouds (PSCs). This is observed in our result through regional depletion of gas phase NO_y reservoirs associated with PSC chemistry ($ClONO_2$, HNO_3, HNO_4) and increases in liquid phase HNO_3 particles and solid phase particles like nitric acid trihydrate (NAT). These changes suggest that PSC chemistry is enhanced, increasing the sedimentation of stratospheric nitrogen compounds and resulting in denitrification of the southern stratosphere. This likely leads to the NO_x and NO_y loss over the south pole. Near the North pole similar responses may occur, but this is hard to discern due to the proximity of the emission sources. Above pressure altitudes of 10 hPa we find areas of stratospheric cooling of up to 0.3 K. This may be contribute to the loss of NO_x and NO_y as it slows down the N to NO_x reformation reactions slow down (Rosenfield and Douglass, 1998). This is unlikely to be the sole driver however, as these NO_x and NO_y responses may be the result of complex interactions between the nitrogen chemistry cycles with the changes in stratospheric temperatures and

https://doi.org/10.5194/egusphere-2024-2866
Preprint. Discussion started: 30 September 2024

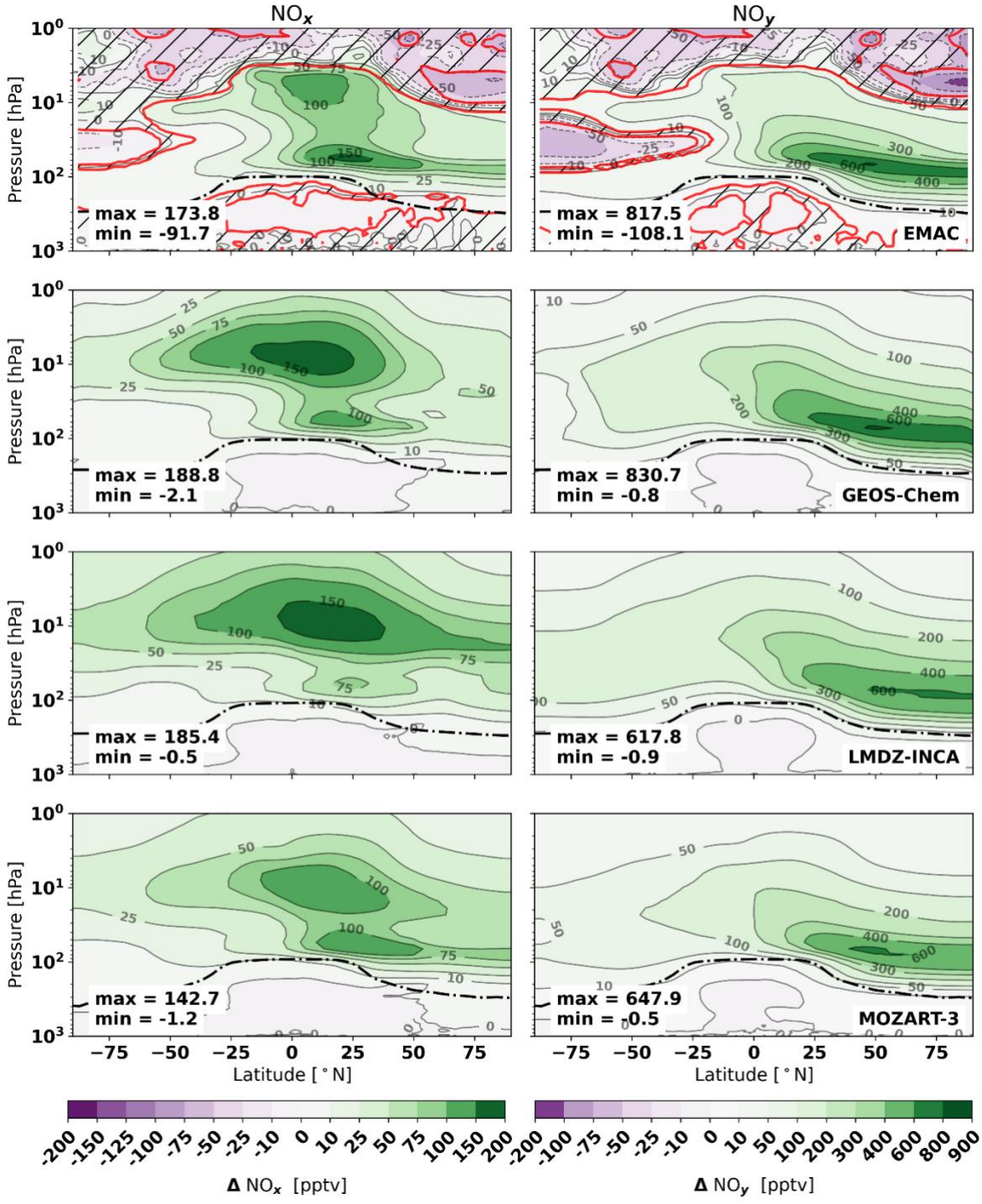

Fig 4: Mean changes in NO_x (left) and NO_y (right) mixing ratios (pptv) in response to the nominal supersonic emissions (A1). Top to bottom: EMAC, GEOS-Chem, LMDZ-INCA, MOZART-3. Hatched areas enclosed by red lines indicate regions which are not statistically significant for the EMAC results. Figures for triple NO_x (A2) and low cruise (A3) in the appendix.

https://doi.org/10.5194/egusphere-2024-2866
Preprint. Discussion started: 30 September 2024

vertical mixing. Both this upper-stratospheric behaviour and the denitrification of the southern hemisphere are not captured by the other models with offline meteorology. Given the importance of NO_x to the O_3 perturbation, the capture of these responses may also affect the O_3 response to emissions. This will be discussed in the next section.

3.4 Ozone

We find similar changes in the stratospheric ozone composition between the models, with ozone loss in the upper-stratosphere and areas of increases in the lower-stratosphere (Fig. 5). The changes in stratospheric H_2O and NO_x affect the ozone concentrations through the HO_x-O_x and NO_x-O_x cycles. The emission of SO_2 forms sulfuric acid which facilitates heterogeneous chemistry, increasing the availability of chlorine and bromine radicals resulting in further ozone depletion. Combined these effects lead to depletion of ozone in the upper-stratosphere paired with increases in the lower-stratosphere from NO_x-driven ozone formation through smog processes or the ozone self-healing effect (Zhang et al. 2023, Eastham et al. 2022, Fritz et al. 2023, Zhang et al. 2021b). This increase is strongest in the LMDZ-INCA model, where the ozone increase spans both hemispheres. In GEOS-Chem and MOZART-3 this increase is limited to the equatorial lower-stratosphere underneath the main lobe of ozone depletion, and this may be driven by the self-healing effect.

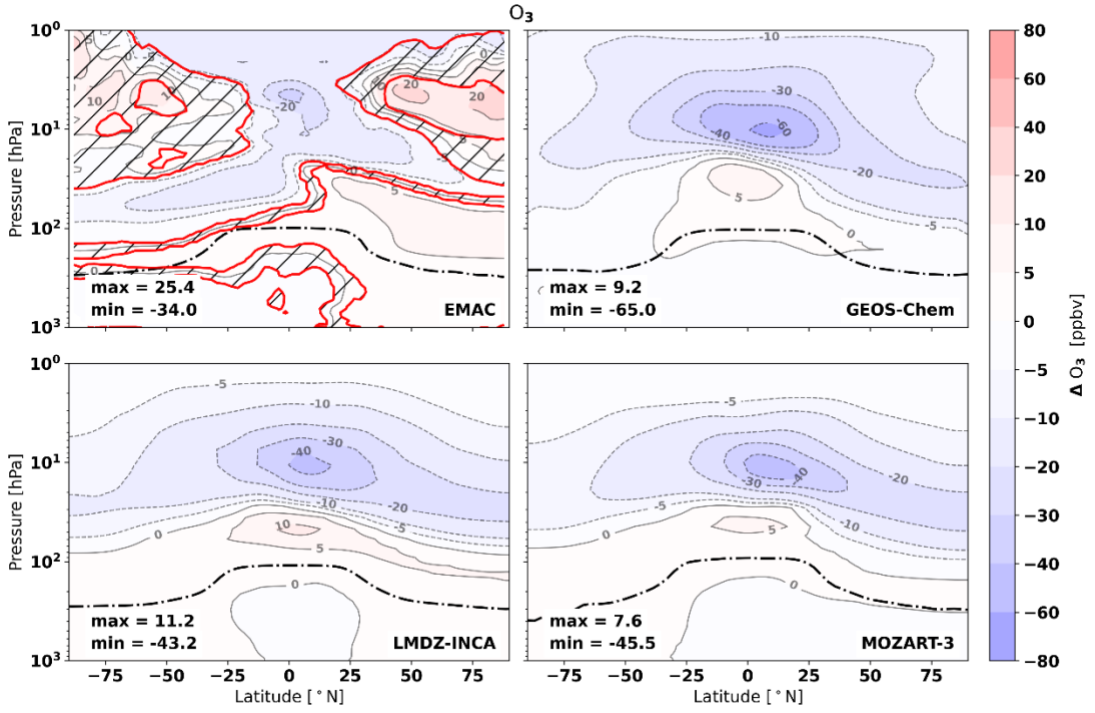

Fig 5: Mean changes in O_3 volume mixing ratios [ppbv] in response to the nominal supersonic (A1) emissions. Hatched areas enclosed by red lines indicate regions which are not statistically significant for the EMAC results. Similar figures for the triple NO_x and low cruise scenarios are provided in the appendix (Fig, A9, A10).

https://doi.org/10.5194/egusphere-2024-2866
Preprint. Discussion started: 30 September 2024

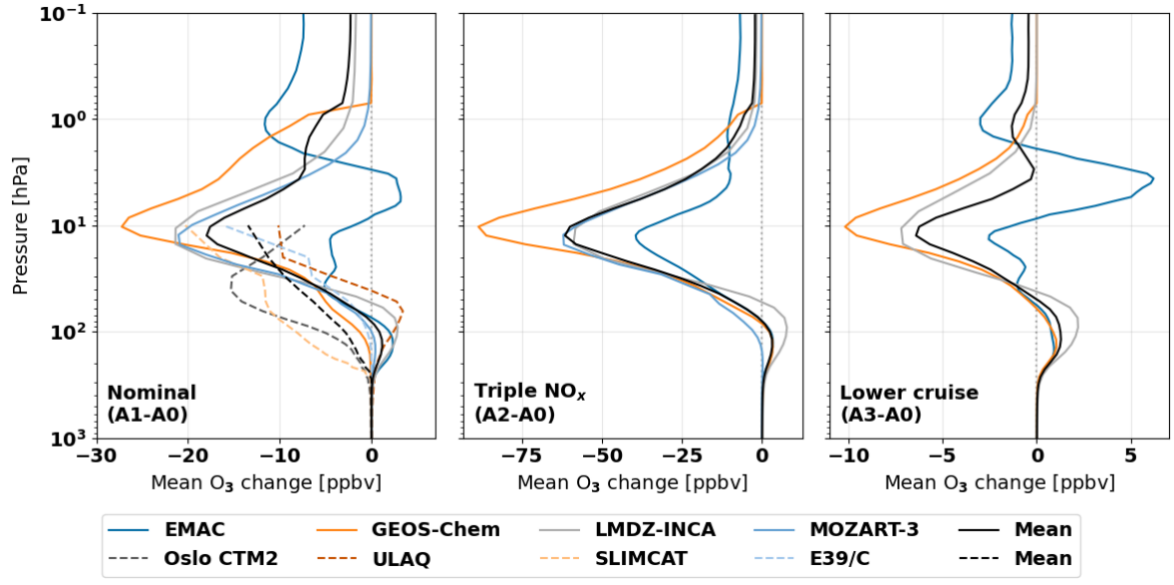

Fig 6: Mean changes in O_3 mixing ratio over altitude for the nominal supersonic (A1, left), triple NO_x (A2, middle) and low cruise (A3, right) emission scenarios. Dashed lines show results from models used by Grewe et al. (2007).

The similarity in ozone responses, particularly between the models with offline meteorology, also extends to the low altitude and triple NO_x perturbation scenarios (Fig 6.). Across all models and scenarios we find increases in lower-stratospheric ozone mixing ratios. Such increases were previously only captured by one of the models used by Grewe et al. (2007), but now they have been observed across multiple recent studies using the GEOS-Chem and WACCM CTMs (Eastham et al. 2022, Zhang et al. 2023; 2021a; 2021b, Kinnison et al. 2020). We expect that this shift in lower-stratospheric responses may be related to overall improvements in the representation of Non-Methane Hydrocarbon (NMHC) chemistry (Houweling et al. 1998). We also observe a shift in the NOy species towards more formation of HNO_3 around the emission areas, reducing the availability of HO_x and NO_x. This may further suppress lower-stratospheric ozone depletion. When NO_x emissions are tripled, the changes in O_3 are enhanced, particularly the loss of O_3 around a pressure altitude of 100 hPa (Fig A9). In the low cruise emissions scenario both the magnitude of ozone increases and losses are reduced considerably (Fig. A10).

Similar to the NO_x and NO_y responses, the O_3 perturbation is different in EMAC than in the other models (Figs. 5, 6). This is likely driven by the inclusion of composition-meteorology feedbacks and online meteorology. The most notable difference is the presence of two lobes of ozone increases at high latitudes above 10 hPa, both of which are partially statistically significant. We hypothesize that their formation is driven by stratospheric cooling and enhancements of PSC chemistry. In the southern hemisphere the latter causes shifts in the abundance of nitrogen and chlorine ($ClONO_2$) reservoir species, which correlate with areas of ozone decreases and increases. In the northern lower stratosphere ozone increase correlates with HNO_3

https://doi.org/10.5194/egusphere-2024-2866
Preprint. Discussion started: 30 September 2024

increase. The patterns that should be associated with PSC chemistry tend to vanish for the triple NO_x emission scenario (Fig A9), which points toward the limited magnitude of PSC processes. The regions of ozone increases around 10 hPa can also be observed in other studies using the EMAC model with online meteorology (Pletzer et al. 2022, Kirner et al. 2014). Kirner et al. (2014) explain the dynamical changes in ozone as a combination of changes in vertical stratospheric transportation and slowdowns of the Chapman mechanism in response to stratospheric cooling. It is likely that these mechanisms also drive part of the dynamical response in the EMAC model, as the increased reduction in the Chapman mechanism can also be observed in the Odd O_x loss rates, which will be evaluated in the next section. Furthermore Kinnison et al. (2020) also demonstrated that the inclusion of interactive dynamics leads to increases in upper-stratospheric ozone formation from supersonic emissions, although their results do not share the characteristics unique to the EMAC model.

We note that there is a nonlinear relationship between the supersonic NO_x emissions and the global O_3 losses across all of the models. In the GEOS-Chem and LMDZ-INCA models the tripling of NO_x emissions increases ozone column losses by factors of 2.39 and 2.56 respectively, whereas these factors are 3.89 and 7.24 for MOZART-3 and EMAC. The high sensitivity of the EMAC model compared to the others is related to the aforementioned differences. Under the triple NO_x emissions EMAC's middle-stratospheric ozone response becomes more similar to that of the other models, leading to more uniform O_3 losses and a large increase in O_3 column losses relative to the nominal scenario. Between the fixed meteorology models MOZART-3 is most sensitive. This may be related to the lower availability of background NO_x in its stratosphere (Table A2), which has been observed when it is used with the ECMWF reanalysis meteorology (Kinnison et al. 2007).

Even though the zonal and vertical averages of the ozone changes are similar across the models, we note that the effects on net column ozone differ between the models over latitude. Fig. 7 shows the mean ozone column change over latitude for the emission scenarios alongside the multi-model mean profile. Across all emission scenarios the disagreement between the models is biggest in the northern hemisphere, with the spread between models increasing towards the north pole. Expanding this into seasonal ozone column changes (Fig. 8) shows that the mean ozone column impacts over the year differs between all models. These differences are particularly notable in polar areas. In EMAC we observe clear increases in northern hemispheric ozone which are strongest in the local winter season, with slight enhancements of southern polar ozone loss from July to November. GEOS-Chem shows enhancement of seasonal ozone loss during both the arctic and Antarctic ozone hole formation, both of which are also slightly present in LMDZ-INCA. In contrast, MOZART-3 finds the highest ozone depletion from June to November in the northern hemisphere. These differences may be indicative of differences in the modelling of PSC processes, but they may also be driven by differences in the availability of stratospheric halogens (Table A4). For example, the enhancement of the ozone hole formation is most visible in GEOS-Chem, which also has the highest background halogen availability. We note the seasonal O_3 column changes of our models also differ from evaluations of a similar emissions scenario using the WACCM6 model by Zhang et al. (2023), who instead find increases in southern hemispheric ozone from September to March with enhanced southern polar losses in-between.

https://doi.org/10.5194/egusphere-2024-2866
Preprint. Discussion started: 30 September 2024

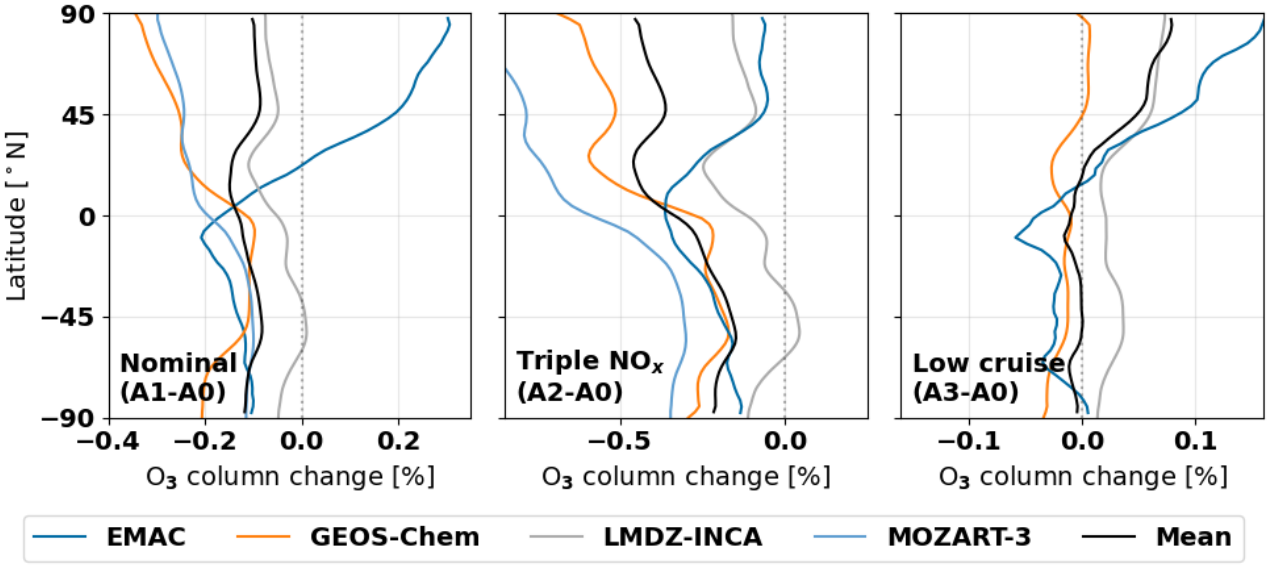

Fig 7: Zonal mean annually averaged changes in O_3 columns for nominal supersonic (A1, left), triple NO_x (A2, middle), and low cruise (A3, right) emission scenarios.

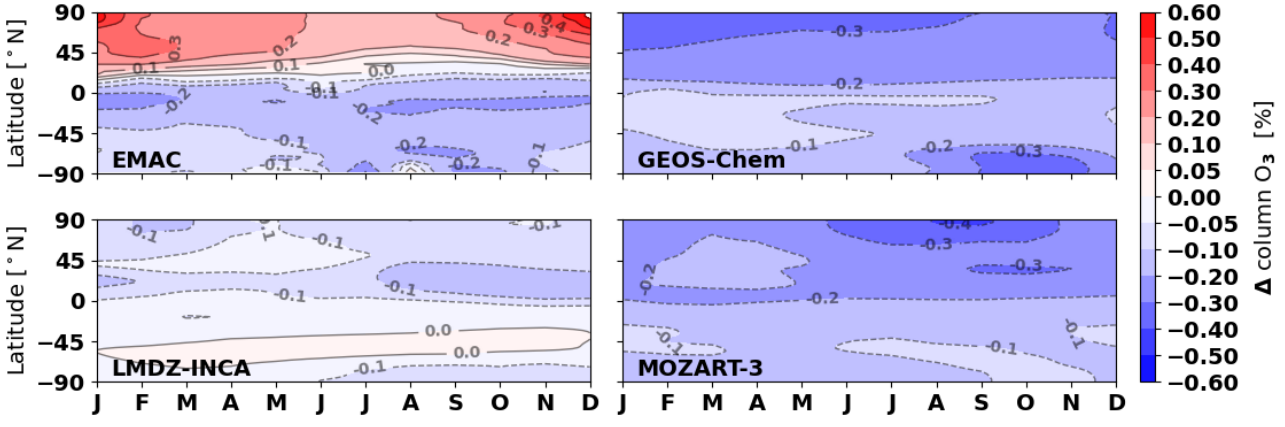

Fig 8: Mean monthly changes in percentage of the ozone columns in response to the nominal supersonic emissions scenario (A1 – A0).

3.5 Odd oxygen loss

To better understand the source of the differences in the ozone responses we evaluate the changes in odd oxygen (O_x) reaction rates for EMAC, GEOS-Chem, and LMDZ-INCA. Across all models the supersonic emissions lead to net-increases in O_x loss. When averaged over altitude the responses are similar across the models (Fig. 9), but the zonal average of the O_x reaction changes also reveals notable differences in the spatial distribution of these loss processes between the model atmospheres (Fig. 10). In the GEOS-Chem and LMDZ-INCA models the increases in O_x losses are primarily driven by increases in NO_x-driven

https://doi.org/10.5194/egusphere-2024-2866
Preprint. Discussion started: 30 September 2024

losses at from 200 to 20 hPa and HO_x-driven losses from 20 hPa to 0.1 hPa (1 hPa for GEOS-Chem). These increases are paired with decreases in O_x-O_x losses, as the availability of O_x reduces from the other loss channels. Across all models we also find an increase in ClO_xBrO_x driven losses above 10 hPa. In the EMAC model the change in NO_x-driven losses is more complex. The zonal average (Fig. 10) shows that this response is more complex due to the presence of areas with reductions in NO_x-driven losses, coinciding with areas of NO_x decreases in the upper-stratosphere and southern hemisphere (Fig. 4). In case of HO_x-driven losses we observe similar decreases around the emission areas in all models, with varying degrees of increases in the upper-stratosphere coinciding, the magnitude of which coincides with the H_2O perturbation lifetimes across the models. For the triple NO_x scenario (A2) we find increased NO_x-driven O_x losses across all models. The enhancement of NO_x-driven O_x loss slightly reduces HO_x and ClO_xBrO_x-driven O_x losses. For the lower cruise altitude scenario (A3) we find similar changes in O_x loss rates as the nominal supersonic scenario but at smaller magnitudes. In the case of the GEOS-Chem and LDMZ-INCA models the reduction in cruise altitude also sharply reduces upper-stratospheric HO_x driven odd O_x losses, resulting from the previously discussed reduction in H_2O perturbation lifetimes.

The changes in ClO_xBrO_x driven losses differ across all of the models, with increases in loss rates being considerably smaller in the LMDZ-INCA model. This difference is likely driven by the differences in halogen availability. Table A4 (SI) shows mean background mixing ratios for key halogens at the surface and from 200 to 10 hPa for the models. Compared to LMDZ-INCA the GEOS-Chem atmosphere has higher availability of all halogens, which may explain its higher ClO_xBrO_x response near the poles. Comparison of surface and stratospheric CFC11 levels suggest that this may be driven by enhanced CFC destruction in GEOS-Chem.

As previously discussed, we see unique characteristics in EMAC's zonal average O_x-loss perturbations due to the inclusion of meteorological feedback. Contrary to the previously shown changes in O_3 and NO_x mixing ratios, the changes in odd O_x loss reactions are statistically significant. The enhancement of PSC chemistry leads to increased southern hemispheric ClO_xBrO_x losses while subsequent denitrification reduces NO_x driven losses in this area. The cooling of the stratosphere also slows the Chapman mechanism, leading to reductions in upper-stratospheric O_x-O_x losses with the exceptions of the areas where there is a net increase of ozone. Combined the inclusion of this feedback leads to differences in the NO_x, NO_y, and O_3 perturbations throughout the stratosphere compared to the models which do not account for it. The incorporation of this feedback may be crucial to adequately assess the impact of high-altitude emissions on the stratospheric composition, especially if the composition of the ozone layer is to be considered. In the consideration of increasing future emissions at high altitudes, whether it be from aviation or spaceflight, the incorporation of meteorological feedbacks may be an important direction for the future development chemistry transport models.

https://doi.org/10.5194/egusphere-2024-2866
Preprint. Discussion started: 30 September 2024

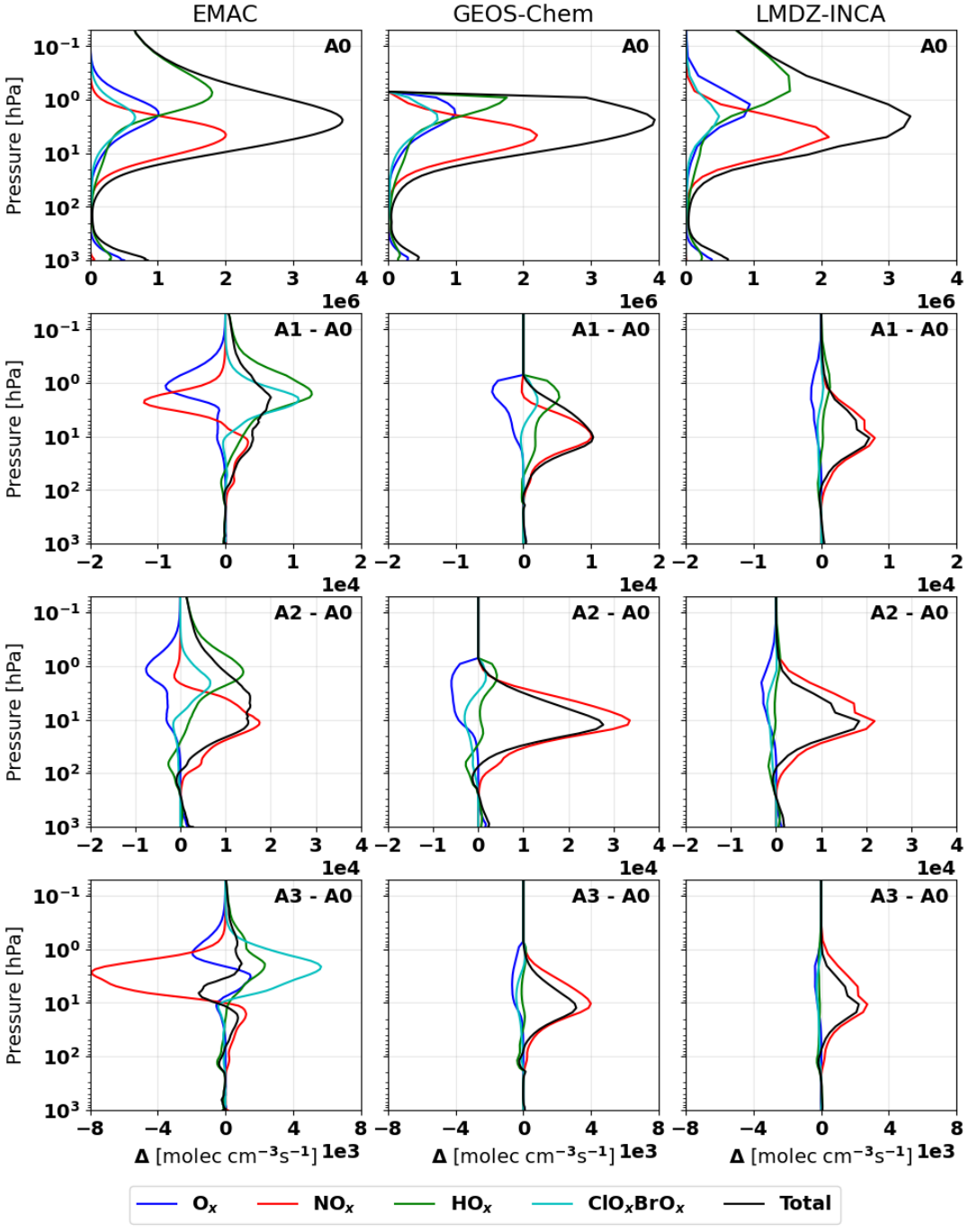

510 **Fig 9: Mean background odd O_x loss rates (top) and odd Ox loss rate perturbations from emission scenarios over pressure altitude for EMAC (left), GEOS-Chem (middle) and LMDZ-INCA (right). From top to bottom: background loss rates, loss rate perturbation from nominal supersonic emissions (A1), loss rate perturbation from triple NOx emissions (A2), loss rate perturbation from low cruise emissions (A3).**

https://doi.org/10.5194/egusphere-2024-2866
Preprint. Discussion started: 30 September 2024

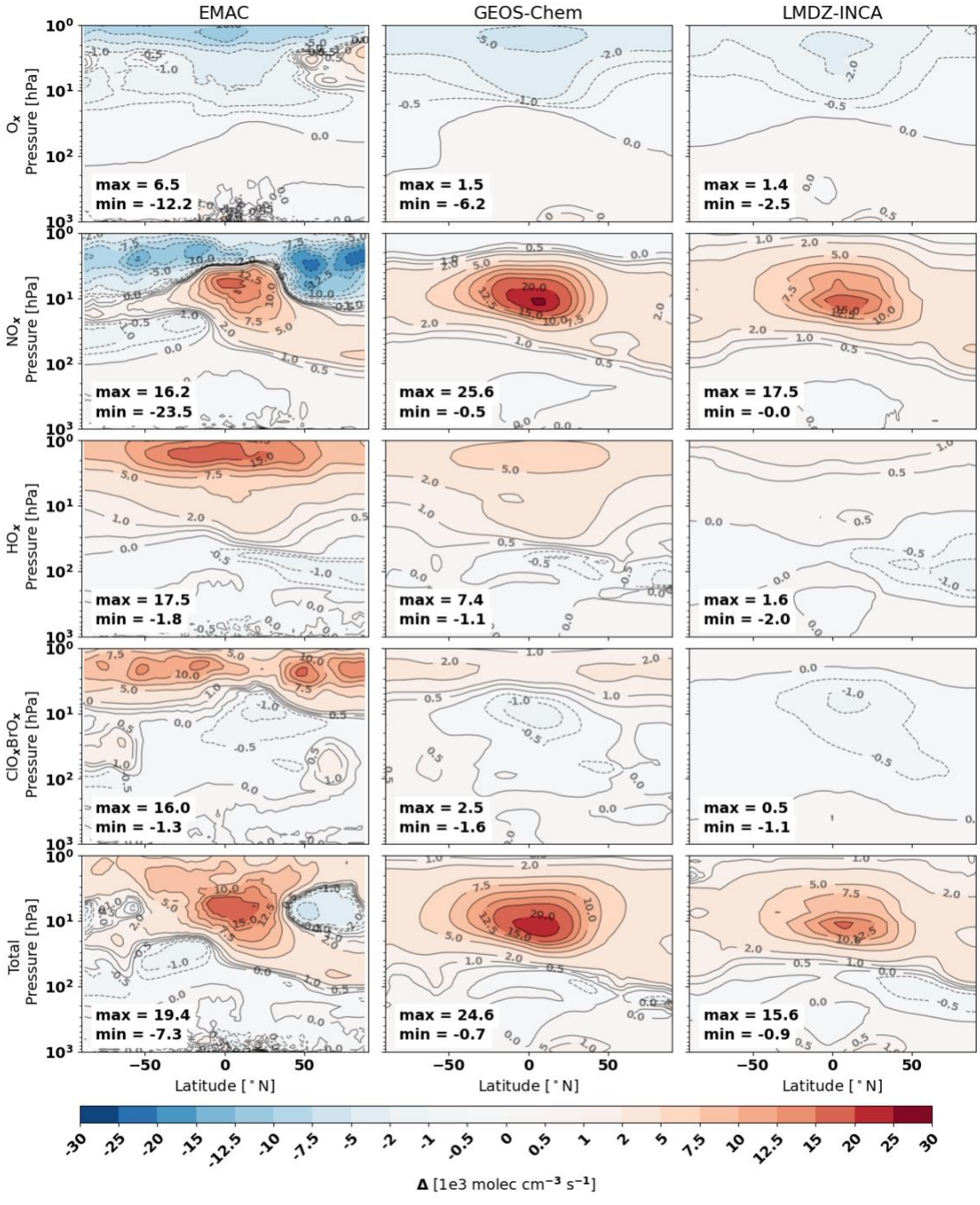

Fig 10: Zonal average mean changes in O_x loss reactions in response to the nominal supersonic emissions for EMAC (left), GEOS-Chem (middle) and LMDZ-INCA (Right). Loss perturbations are split into O_x-driven loss (top), NO_x-driven loss (second row), HO_x-driven loss (third), ClO_xBrO_x driven loss (fourth) and total changes in odd O_x loss (bottom). Values in molec cm^{-3} s^{-1}. Similar figures for the triple NO_x (A2) and low cruise (A3) scenarios are provided in the SI.

https://doi.org/10.5194/egusphere-2024-2866
Preprint. Discussion started: 30 September 2024

We use the same O_x loss reaction grouping as Zhang et al. (2021b) to facilitate comparison with their results. Overall, we find agreement in background loss rates across the models (Fig. 9), with LMDZ-INCA having slightly smaller overall O_x loss rates. Our background loss rates, in particular those of the GEOS-Chem model, also closely match loss rates from the WACCM4 model as reported by Zhang et al. (2021b). The most notable difference between the models occurs above 1 hPa, which marks the upper boundary of GEOS-Chem's stratospheric chemistry domain. Above this altitude GEOS-Chem has no O_x chemistry, yet other species related to ozone chemistry are allowed to evolve freely. This may lead to an accumulation of excessive HO_x, which then leads to excessive HO_x-driven O_x loss when it is transported downwards into the region of O_x chemistry. This may be what drives the stronger HO_x-O_x losses in the GEOS-Chem model, and it may contribute to the higher O_3 loss in GEOS-Chem from 5 to 1 hPa compared to the MOZART-3 and LMDZ-INCA models. Similar emission scenarios to our nominal supersonic and triple NO_x scenarios were also studied by Zhang et al. (2021b) using WACCM4. Our results agree well with their evaluations. We note a strong similarity in the changes in odd O_x losses between GEOS-Chem and WACCM4 for the nominal supersonic (A1) and triple NO_x (A2) and comparable scenarios (Case A & C, Zhang et al. 2021b). The overall magnitude of changes in loss rates is lower in GEOS-Chem, but we find similar vertical profiles across all loss rate families up to 1 hPa.

3.6 Modelling considerations

In the previous sections we have identified some notable differences between the models which we use in this study. Here we summarize the most important differences between the model and their effects, as they may provide fruitful directions for further development of these models and future work which aims to utilize them.

Earlier works have identified that the accumulation of stratospheric H_2O plays a key role in the climate impact of supersonic aviation (Zhang et al. 2023, Eastham et al. 2022, Matthes et al. 2022, Grewe et al. 2007). In our results we find indications that the accumulation of stratospheric H_2O and its distribution across hemispheres may be related to the vertical and horizontal model resolutions, which affect the modelling of critical transport processes. The use of higher vertical resolutions may lead to higher stratospheric H_2O perturbation lifetimes and higher horizontal resolutions reduce interhemispheric mixing. The link between vertical resolution and perturbation lifetime may be strengthened by the use of fixed tropospheric H_2O mixing ratios in the LMDZ-INCA and GEOS-Chem models. In these cases, the troposphere acts as a sink for stratospheric H_2O emissions, which may lead to underestimation of perturbation lifetimes for lower-stratospheric emissions. Combined, this explains why we don't see the same level of improvement in model agreement for H_2O perturbations as we see for O_3 compared to the results of Grewe et al. (2007). We expect that the adoption of a common vertical grid and resolution may remove a factor contributing to model disagreement of stratospheric H_2O perturbation lifetimes, and this may therefore be desirable in future multi-model studies. Improvements in model agreement does not necessarily indicate better model performance however, for this validation with observations and measurements remains to be crucial.

https://doi.org/10.5194/egusphere-2024-2866
Preprint. Discussion started: 30 September 2024

With regards to the ozone impact, we find considerable improvement in model agreement compared to the previous multi-model assessment by Grewe et al. (2007). Between the models with offline meteorology the biggest difference is identified in the GEOS-Chem model, which has a lower upper altitude for its stratospheric ozone chemistry than all other models (Eastham et al. 2014). Above this limit species such as HO_x still evolve freely in the model's mesosphere, and we expect this may result in excessive influx of HO_x at the upper-stratospheric boundary. Ultimately, our findings do not indicate that this has an effect on the observed changes in the total ozone columns for the supersonic emission scenarios. It may however become a more relevant restriction for the study of the effects of higher altitude emissions, such as from hypersonic vehicles or spaceflight.

Finally, we find that the use of online meteorology in the EMAC model has considerable effects on the impact of all supersonic emission scenarios. This is particularly influential for the accumulation of stratospheric nitrogen compounds, and by extend it also affects the changes in global ozone distribution due to the emissions. Notably, the inclusion of chemistry-meteorological feedback allowed EMAC to observe some interactions overlooked by the other models such as the denitrification of the southern stratosphere due to enhancements of PSC chemistry from stratospheric cooling. A downside of the use of online meteorology is that it makes models more susceptible to noise, requiring longer model integration times to ensure results are statistically significant. This is less practical than working with offline meteorology, but our results indicate that some critical interactions may be overlooked otherwise. Therefore, we recommend that the effect of chemistry-meteorology feedback is considered and explored further in future studies regarding the impact of high-altitude emissions.

4 Conclusions

For the first time in about eighteen years, we present a comprehensive review of the effects of supersonic aviation on the stratospheric composition of a future atmosphere as calculated by four widely-used state-of-the-art chemistry transport models. We use the EMAC, LMDZ-INCA, GEOS-Chem, and MOZART-3 models to make an updated assessment of the emission scenarios of the SCENIC project (Grewe et al. 2007) to evaluate the effects of advancements in atmospheric chemistry and modelling since then. In this scenario we consider the adoption of a Mach 2 supersonic aircraft operating at cruise altitudes of 16.5 to 19.5 km that partially replaces subsonic aviation traffic. We also evaluate two variants of this scenario. One considers increased NO_x emissions that are more comparable to modern emission estimates for supersonic vehicles. The other considers a lower cruise speed (Mach 1.6) and altitude instead (13.1 to 16.7 km).

In the nominal supersonic emission scenario, the partial replacement of subsonic traffic with supersonic vehicles leads to substantial accumulation of stratospheric water vapor (H_2O) which is often associated with positive radiative forcing. This accumulation is contained almost entirely within the lower altitudes of the northern stratosphere, yielding a model-mean perturbation of +61.34 Tg with a spread of +20.14 to +116.53 Tg. This value closely agrees with estimates from the earlier assessment of the SCENIC scenario, but we find a larger spread in perturbation masses. We expect that this originates from

https://doi.org/10.5194/egusphere-2024-2866
Preprint. Discussion started: 30 September 2024

differences in H_2O perturbation lifetime, which are primarily driven by differences in vertical model resolutions and the treatment of tropospheric water vapour. The H_2O perturbation lifetime may be a function of the vertical model resolution, and low resolutions may lead to excessive removal of stratospheric H_2O emissions. This is most influential in the low cruise altitude emissions, where we find reduced model-mean H_2O increases of +9.34 Tg with a range of +2.37 to +19.69 Tg. This is paired with large reductions in H_2O perturbation lifetimes which depend on vertical model resolution. We also find that the use of higher horizontal resolutions reduced interhemispheric transport of the H_2O perturbation in current models compared to the previous assessment of these scenarios.

In most cases the supersonic emissions lead to loss of the global ozone column, driven by depletion of middle- and upper-stratospheric ozone paired with lower-stratospheric increases, of smaller magnitude. For the nominal emissions scenario we find a model-average decrease in the global ozone column of -0.11%, with a range of -0.22% to +0.03%. Compared to the earlier multi-model assessment of the SCENIC project we find considerable improvements in the agreement of the ozone perturbation across the models, which may be indicative of substantial improvements in the modelling of ozone chemistry. The ozone response is primarily driven by the emission of NO_x, followed by sulfur emissions and then H_2O, leading to lower-stratospheric ozone increases and upper-stratospheric losses. Consequently, we find that in the scenario with triple the supersonic NO_x emissions the global column ozone loss increases to -0.31%, ranging between -0.57% to -0.09%. The increase in global ozone losses is not linearly tied to the supersonic NO_x emissions, and we find that the degree of nonlinearity varies across models. When a low cruise altitude is used, the ozone impact is strongly reduced, yielding a net-increase in the global ozone column of +0.02% instead (range -0.01% to +0.04%).

The adoption of a lower cruise speed and altitude sharply reduces the impacts of supersonic emissions on atmospheric composition. It leads to reductions in the perturbations of stratospheric O_3, NO_y, H_2O, and aerosol loadings, which will implicitly also reduce the effect on radiative forcing. Limitations on cruise altitude and speed may prove to be the most effective means to minimize the environmental impact of a future supersonic fleet. The impact on the distribution of atmospheric ozone in particular may be further reduced by the reduction of fleetwide NO_x emissions.

Finally, we find that the use of online meteorology in the EMAC model leads to differences in the assessment of high-altitude emissions compared to the other models. In EMAC, the introduction of supersonic emissions lead to a cooling of the stratosphere. This enhances PSC formation in the southern hemisphere, increasing the availability of halogens for heterogeneous chemistry and contributing to denitrification of the southern hemisphere through sedimentation of PSC particles. These effects lead to a loss of ozone in the southern mid-stratosphere which is not captured by the models with offline meteorology. At the upper model domain above 10 hPa the slowing of the Chapman mechanism and changes in vertical mixing lead to a complex upper-stratospheric ozone response, including areas of ozone increases. These interactions are not captured by other models with offline meteorology, but they have considerable consequences for the impact of high-altitude emissions.

https://doi.org/10.5194/egusphere-2024-2866
Preprint. Discussion started: 30 September 2024

From this we identify that the inclusion of such feedback may be of necessary to adequately capture the effects of high-altitude emissions on the stratosphere. This is particularly true for changes in ozone chemistry, and it may prove a fruitful direction for future developments in chemistry transport models.

5 Acknowledgements

This work was funded by the European Union's Horizon 2020 research and innovation programme. Authors (J.A.H, R.T., J.P., V.G., D.H., I.C.D., M.M.M.) were funded by the MORE & LESS project (MDO and REgulations for Low-boom Environmentally Sustainable Supersonic aviation, grant No. 101006856). Others (A.S. & S.M.) were funded by the SENECA project ((LTO) Noise and Emissions of Supersonic Aircraft, grant No.101006742). The GEOS-Chem simulations were supported by the Dutch national e-infrastructure and supercomputer with the support of the SURF Cooperative (Grant no. EINF-5945). The EMAC model simulations were computed at the German Climate Computing Center (DKRZ). The resources for the simulations were provided by the German Bundesministerium für Bildung und Forschung (BMBF).

6 Data availability

The data supporting the results of this work is publicly available at DOI: **10.4121/dd38833d-6c5d-47d8-bb10-7535ce1eecf1** (van 't Hoff et al. 2024b). Reserved DOI, dataset to be minted on acceptance. Reviewers can preview the dataset through https://data.4tu.nl/private_datasets/_qffTJdRitRConukkBmBTegk9CJTJZD36xRUN6lif5M

7 Author contribution

Conceptualization: ICD, VG, DH, JAH, RNT; Formal analysis: DH, JAH, JP, AS; Investigation: ICD, VG, DH, JAH, SM, JP, AS; Data Curation: DH, JAH, MMM, JP, AS, RNT; Writing - Original Draft: JAH; Writing - Review & Editing: all; Visualization: JAH, JP; Supervision: ICD; Funding acquisition: ICD, VG, DH, SM, AS.

8 Competing interests

The authors declare that they have no conflict of interest.

References

Matthes, S., Lee, D. S., De Leon, R. R., Lim, L., Owen, B., Skowron, A., Thor, R. N., and Terrenoire, E.: Review: The Effects of Supersonic Aviation on Ozone and Climate, Aerospace, 9, 41, https://doi.org/10.3390/aerospace9010041, 2022.

https://doi.org/10.5194/egusphere-2024-2866
Preprint. Discussion started: 30 September 2024

Berton, J. J., Huff, D. L., Geiselhart, K., and Seidel, J.: Supersonic Technology Concept Aeroplanes for Environmental Studies, in: AIAA Scitech 2020 Forum, American Institute of Aeronautics and Astronautics, https://doi.org/10.2514/6.2020-0263, 2020.

Solomon, S.: Stratospheric ozone depletion: A review of concepts and history, 1999.

Johnston, H.: Reduction of stratospheric ozone by nitrogen oxide catalysts from supersonic transport exhaust, Science, 173, 517–522, 1971.

Pitari, G., Aquila, V., Kravitz, B., Robock, A., Watanabe, S., Cionni, I., De Luca, N., Di Genova, G., Mancini, E., and Tilmes, S.: Stratospheric ozone response to sulfate geoengineering: Results from the Geoengineering Model Intercomparison Project (GeoMIP), Journal of Geophysical Research, 119, 2629–2653, https://doi.org/10.1002/2013jd020566, 2014.

Granier, C. and Brasseur, G.: Impact of heterogeneous chemistry on model predictions of ozone changes, Journal of Geophysical Research: Atmospheres, 97, 18015–18033, https://doi.org/10.1029/92JD02021, 1992.

Zhang, J., Wuebbles, D., Kinnison, D., and Baughcum, S. L.: Stratospheric Ozone and Climate Forcing Sensitivity to Cruise Altitudes for Fleets of Potential Supersonic Transport Aircraft, Journal of Geophysical Research: Atmospheres, 126, https://doi.org/10.1029/2021jd034971, 2021a.

Zhang, J., Wuebbles, D., Kinnison, D., and Baughcum, S. L.: Potential Impacts of Supersonic Aircraft Emissions on Ozone and Resulting Forcing on Climate: An Update on Historical Analysis, Journal of Geophysical Research: Atmospheres, 126, https://doi.org/10.1029/2020JD034130, 2021b.

Speth, R. L., Eastham, S. D., Fritz, T. M., Sanz-Morére, I., Agarwal, A., Prashanth, P., Allroggen, F., and Barrett, S. R. H.: Global Environmental Impact of Supersonic Cruise Aircraft in the Stratosphere, 2021.

Crutzen, P. J.: SST's: A Threat to the Earth's Ozone Shield, Ambio, 1, 41–51, 1972.

van 't Hoff, J.A., Grewe V., and Dedoussi I.C.: Sensitivities of atmospheric ozone and radiative forcing to supersonic aircraft emissions across two flight corridors. Journal of Geophysical Research: Atmospheres, 2024a (under review).

Eastham, S. D., Weisenstein, D. K., Keith, D. W., and Barrett, S. R. H.: Quantifying the impact of sulfate geoengineering on mortality from air quality and UV-B exposure, Atmospheric Environment, 187, 424–434, https://doi.org/10.1016/j.atmosenv.2018.05.047, 2018.

Pletzer, J., Hauglustaine, D., Cohen, Y., Jöckel, P., and Grewe, V.: The climate impact of hydrogen-powered hypersonic transport, Atmospheric Chemistry and Physics, 22, 14323–14354, https://doi.org/10.5194/acp-22-14323-2022, 2022.

Lee, D. S., Fahey, D. W., Skowron, A., Allen, M. R., Burkhardt, U., Chen, Q., Doherty, S. J., Freeman, S., Forster, P. M., Fuglestvedt, J., Gettelman, A., De León, R. R., Lim, L. L., Lund, M. T., Millar, R. J., Owen, B., Penner, J. E., Pitari, G., Prather, M. J., Sausen, R., and Wilcox, L. J.: The contribution of global aviation to anthropogenic climate forcing for 2000 to 2018, Atmospheric Environment, 244, https://doi.org/10.1016/j.atmosenv.2020.117834, 2021.

Stenke, A., Grewe, V., and Pechtl, S.: Do supersonic aircraft avoid contrails?, 2008.

Grewe, V., Stenke, A., Ponater, M., Sausen, R., Pitari, G., Iachetti, D., Rogers, H., Dessens, O., Pyle, J., Isaksen, I. S. A., Gulstad, L., Søvde, O. A., Marizy, C., and Pascuillo, E.: Climate impact of supersonic air traffic: an approach to optimize a potential future supersonic fleet – results from the EU-project SCENIC, Atmospheric Chemistry and Physics, 7, 5129–5145, https://doi.org/10.5194/acp-7-5129-2007, 2007.

IPCC: Special report on aviation and the global atmosphere, edited by: Penner, J. E., Lister, D. H., Griggs, D. J., Dokken, D. J., and McFarland, M., Intergovernmental Panel on Climate Change, 1999.

Grewe, V., Plohr, M., Cerino, G., Di Muzio, M., Deremaux, Y., Galerneau, M., de Saint Martin, P., Chaika, T., Hasselrot, A., Tengzelius, U., and Korovkin, V. D.: Estimates of the climate impact of future small-scale supersonic transport aircraft-results from the HISAC EU-project, 2010.

https://doi.org/10.5194/egusphere-2024-2866
Preprint. Discussion started: 30 September 2024

Pletzer, J. and Grewe, V.: Sensitivities of atmospheric composition and climate to altitude and latitude of hypersonic aircraft emissions, Atmospheric Chemistry and Physics, 24, 1743–1775, https://doi.org/10.5194/acp-24-1743-2024, 2024.

Eastham, S. D., Fritz, T., Sanz-Morère, I., Prashanth, P., Allroggen, F., Prinn, R. G., Speth, R. L., and Barrett, S. R. H.: Impacts of a near-future supersonic aircraft fleet on atmospheric composition and climate, Environmental Science: Atmospheres, https://doi.org/10.1039/d1ea00081k, 2022.

Kawa, S. R., Anderson, J. G., Baughcum, S. L., Brock, C. A., Brune, W. H., Cohen, R. C., Kinnison, D. E., Newman, P. A., Rodriquez, J. M., and Stolarski, R. S.: Assessment of the effects of high-speed aircraft in the stratosphere: 1998, 1999.

Pitari, G., Iachetti, D., Mancini, E., Montanaro, V., De Luca, N., Marizy, C., Dessens, O., Rogers, H., Pyle, J., Grewe, V., Stenke, A., and Søvde, O. A.: Radiative forcing from particle emissions by future supersonic aircraft, Atmospheric Chemistry and Physics, 8, 4069–4084, https://doi.org/10.5194/acp-8-4069-2008, 2008.

Riahi, K., van Vuuren, D. P., Kriegler, E., Edmonds, J., O'Neill, B. C., Fujimori, S., Bauer, N., Calvin, K., Dellink, R., Fricko, O., Lutz, W., Popp, A., Cuaresma, J. C., Kc, S., Leimbach, M., Jiang, L., Kram, T., Rao, S., Emmerling, J., Ebi, K., Hasegawa, T., Havlik, P., Humpenöder, F., Da Silva, L. A., Smith, S., Stehfest, E., Bosetti, V., Eom, J., Gernaat, D., Masui, T., Rogelj, J., Strefler, J., Drouet, L., Krey, V., Luderer, G., Harmsen, M., Takahashi, K., Baumstark, L., Doelman, J. C., Kainuma, M., Klimont, Z., Marangoni, G., Lotze-Campen, H., Obersteiner, M., Tabeau, A., and Tavoni, M.: The Shared Socioeconomic Pathways and their energy, land use, and greenhouse gas emissions implications: An overview, Global Environmental Change, 42, 153–168, https://doi.org/10.1016/j.gloenvcha.2016.05.009, 2017.

Grewe, V. and Stenke, A.: AirClim: An efficient tool for climate evaluation of aircraft technology, Atmospheric Chemistry and Physics, 8, 4621–4639, https://doi.org/10.5194/acp-8-4621-2008, 2008.

Jöckel, P., Tost, H., Pozzer, A., Kunze, M., Kirner, O., Brenninkmeijer, C. A. M., Brinkop, S., Cai, D. S., Dyroff, C., Eckstein, J., Frank, F., Garny, H., Gottschaldt, K.-D., Graf, P., Grewe, V., Kerkweg, A., Kern, B., Matthes, S., Mertens, M., Meul, S., Neumaier, M., Nützel, M., Oberländer-Hayn, S., Ruhnke, R., Runde, T., Sander, R., Scharffe, D., and Zahn, A.: Earth System Chemistry integrated Modelling (ESCiMo) with the Modular Earth Submodel System (MESSy) version 2.51, Geoscientific Model Development, 9, 1153–1200, https://doi.org/10.5194/gmd-9-1153-2016, 2016.

The MESSy Consortium. (2021). The Modular Earth Submodel System (2.55.2). Zenodo. https://doi.org/10.5281/zenodo.8360276

Roeckner, E., Bäuml, G., Bonaventura, L., Brokopf, R., Esch, M., Giorgetta, M., Hagemann, S., Kirchner, I., Kornblueh, L., Manzini, E., Rhodin, A., Schlese, U., Schulzweida, U., and Tompkins, A.: The atmospheric general circulation model ECHAM 5. PART I: Model description, https://doi.org/10.17617/2.995269, 2003.

Sander, R., Baumgaertner, A., Gromov, S., Harder, H., Jöckel, P., Kerkweg, A., Kubistin, D., Regelin, E., Riede, H., Sandu, A., Taraborrelli, D., Tost, H., and Xie, Z.-Q.: The atmospheric chemistry box model CAABA/MECCA-3.0, Geoscientific Model Development, 4, 373–380, https://doi.org/10.5194/gmd-4-373-2011, 2011.

Eastham, S., Long, M., Keller, C., Lundgren, E., Yantosca, R., Zhuang, J., Li, C., Lee, C., Yannetti, M., Auer, B., Clune, T., Kouatchou, J., Putman, W., Thompson, M., Trayanov, A., Molod, A., Martin, R., and Jacob, D.: GEOS-Chem High Performance (GCHP v11-02c): a next-generation implementation of the GEOS-Chem chemical transport model for massively parallel applications, Geoscientific Model Development, 11, 2941–2953, https://doi.org/10.5194/gmd-11-2941-2018, 2018.

Eastham, S. D., Weisenstein, D. K., and Barrett, S. R. H.: Development and evaluation of the unified tropospheric–stratospheric chemistry extension (UCX) for the global chemistry-transport model GEOS-Chem, Atmospheric Environment, 89, 52–63, https://doi.org/10.1016/j.atmosenv.2014.02.001, 2014.

The International GEOS-Chem User Community: geoschem/GCHP: GCHP 14.1.1, , https://doi.org/10.5281/zenodo.7696683, 2023.

https://doi.org/10.5194/egusphere-2024-2866
Preprint. Discussion started: 30 September 2024

Hauglustaine, D. A., Hourdin, F., Jourdain, L., Filiberti, M.-A., Walters, S., Lamarque, J.-F., and Holland, E. A.: Interactive chemistry in the Laboratoire de Météorologie Dynamique general circulation model: Description and background tropospheric chemistry evaluation, Journal of Geophysical Research: Atmospheres, 109, 2004.

Hauglustaine, D. A., Balkanski, Y., and Schulz, M.: A global model simulation of present and future nitrate aerosols and their direct radiative forcing of climate, Atmospheric Chemistry and Physics, 14, 11031–11063, 2014.

Terrenoire, E., Hauglustaine, D. A., Cohen, Y., Cozic, A., Valorso, R., Lefèvre, F., and Matthes, S.: Impact of present and future aircraft NO_x and aerosol emissions on atmospheric composition and associated direct radiative forcing of climate, Atmospheric Chemistry and Physics, 22, 11987–12023, https://doi.org/10.5194/acp-22-11987-2022, 2022.

Kinnison, D. E., Brasseur, G. P., Walters, S., Garcia, R. R., Marsh, D. R., Sassi, F., Harvey, V. L., Randall, C. E., Emmons, L., Lamarque, J. F., Hess, P., Orlando, J. J., Tie, X. X., Randel, W., Pan, L. L., Gettelman, A., Granier, C., Diehl, T., Niemeier, U., and Simmons, A. J.: Sensitivity of chemical tracers to meteorological parameters in the MOZART-3 chemical transport model, Journal of Geophysical Research: Atmospheres, 112, https://doi.org/10.1029/2006JD007879, 2007.

Skowron, A., Lee, D. S., De León, R. R., Lim, L. L., and Owen, B.: Greater fuel efficiency is potentially preferable to reducing NOx emissions for aviation's climate impacts, Nat Commun, 12, 564, https://doi.org/10.1038/s41467-020-20771-3, 2021.

Kirner, O., Ruhnke, R., Buchholz-Dietsch, J., Jöckel, P., Brühl, C., and Steil, B.: Simulation of polar stratospheric clouds in the chemistry-climate-model EMAC via the submodel PSC, Geoscientific Model Development, 4, 169–182, https://doi.org/10.5194/gmd-4-169-2011, 2011.

Jöckel, P., Kerkweg, A., Pozzer, A., Sander, R., Tost, H., Riede, H., Baumgaertner, A., Gromov, S., and Kern, B.: Development cycle 2 of the modular earth submodel system (MESSy2), Geoscientific Model Development, 3, 717–752, 2010.

Burkholder, J. B., Sander, S. P., Abbatt, J. P. D., Barker, J. R., Cappa, C., Crounse, J. D., Dibble, T. S., Huie, R. E., Kolb, C. E., Kurylo, M. J., Orkin, V. L., Percival, C. J., Wilmouth, D. M., and Wine, P. H.: Chemical kinetics and photochemical data for use in atmospheric studies; evaluation number 19, 2020.

Kunze, M., Godolt, M., Langematz, U., Grenfell, J. L., Hamann-Reinus, A., and Rauer, H.: Investigating the early Earth faint young Sun problem with a general circulation model, Planetary and Space Science, 98, 77–92, https://doi.org/10.1016/j.pss.2013.09.011, 2014.

Dietmüller, S., Jöckel, P., Tost, H., Kunze, M., Gellhorn, C., Brinkop, S., Frömming, C., Ponater, M., Steil, B., Lauer, A., and Hendricks, J.: A new radiation infrastructure for the Modular Earth Submodel System (MESSy, based on version 2.51), Geoscientific Model Development, 9, 2209–2222, https://doi.org/10.5194/gmd-9-2209-2016, 2016.

Bey, I., Jacob, D. J., Yantosca, R. M., Logan, J. A., Field, B. D., Fiore, A. M., Li, Q., Liu, H. Y., Mickley, L. J., and Schultz, M. G.: Global modeling of tropospheric chemistry with assimilated meteorology: Model description and evaluation, Journal of Geophysical Research: Atmospheres, 106, 23073–23095, 2001.

Damian, V., Sandu, A., Damian, M., Potra, F., and Carmichael, G. R.: The kinetic preprocessor KPP-a software environment for solving chemical kinetics, Computers & Chemical Engineering, 26, 1567–1579, 2002.

Bian, H. and Prather, M. J.: Fast-J2: Accurate simulation of stratospheric photolysis in global chemical models, Journal of Atmospheric Chemistry, 41, 281–296, 2002.

Fritz, T. M., Dedoussi, I. C., Eastham, S. D., Speth, R. L., Henze, D. K., and Barrett, S. R. H.: Identifying the ozone-neutral aircraft cruise altitude, Atmospheric Environment, 276, 119057, https://doi.org/10.1016/j.atmosenv.2022.119057, 2022.

https://doi.org/10.5194/egusphere-2024-2866
Preprint. Discussion started: 30 September 2024

Keller, C. A., Knowland, K. E., Duncan, B. N., Liu, J., Anderson, D. C., Das, S., Lucchesi, R. A., Lundgren, E. W., Nicely, J. M., Nielsen, E., Ott, L. E., Saunders, E., Strode, S. A., Wales, P. A., Jacob, D. J., and Pawson, S.: Description of the NASA GEOS Composition Forecast Modeling System GEOS-CF v1.0, J Adv Model Earth Syst, 13, e2020MS002413, https://doi.org/10.1029/2020MS002413, 2021.

Gelaro, R., McCarty, W., Suárez, M. J., Todling, R., Molod, A., Takacs, L., Randles, C. A., Darmenov, A., Bosilovich, M. G., Reichle, R., Wargan, K., Coy, L., Cullather, R., Draper, C., Akella, S., Buchard, V., Conaty, A., da Silva, A. M., Gu, W., Kim, G.-K., Koster, R., Lucchesi, R., Merkova, D., Nielsen, J. E., Partyka, G., Pawson, S., Putman, W., Rienecker, M., Schubert, S. D., Sienkiewicz, M., and Zhao, B.: The Modern-Era Retrospective Analysis for Research and Applications, Version 2 (MERRA-2), Journal of Climate, 30, 5419–5454, https://doi.org/10.1175/JCLI-D-16-0758.1, 2017.

Carn, S. A., Yang, K., Prata, A. J., and Krotkov, N. A.: Extending the long-term record of volcanic SO2 emissions with the Ozone Mapping and Profiler Suite nadir mapper, Geophysical Research Letters, 42, 925–932, https://doi.org/10.1002/2014GL062437, 2015.

Hourdin, F., Rio, C., Grandpeix, J.-Y., Madeleine, J.-B., Cheruy, F., Rochetin, N., Jam, A., Musat, I., Idelkadi, A., and Fairhead, L.: LMDZ6A: The atmospheric component of the IPSL climate model with improved and better tuned physics, Journal of Advances in Modeling Earth Systems, 12, e2019MS001892, 2020.

Boucher, O., Servonnat, J., Albright, A. L., Aumont, O., Balkanski, Y., Bastrikov, V., Bekki, S., Bonnet, R., Bony, S., and Bopp, L.: Presentation and evaluation of the IPSL-CM6A-LR climate model, Journal of Advances in Modeling Earth Systems, 12, e2019MS002010, 2020.

Van Leer, B.: Towards the ultimate conservative difference scheme. IV. A new approach to numerical convection, Journal of Computational Physics, 23, 276–299, 1977.

Hourdin, F. and Armengaud, A.: The use of finite-volume methods for atmospheric advection of trace species. Part I: Test of various formulations in a general circulation model, Monthly Weather Review, 127, 822–837, 1999.

Emanuel, K. A.: A scheme for representing cumulus convection in large-scale models, Journal of the atmospheric sciences, 48, 2313–2329, 1991.

Folberth, G. A., Hauglustaine, D. A., Lathière, J., and Brocheton, F.: Interactive chemistry in the Laboratoire de Météorologie Dynamique general circulation model: model description and impact analysis of biogenic hydrocarbons on tropospheric chemistry, Atmospheric Chemistry and Physics, 6, 2273–2319, 2006.

Lefevre, F., Brasseur, G. P., Folkins, I., Smith, A. K., and Simon, P.: Chemistry of the 1991–1992 stratospheric winter: Three-dimensional model simulations, Journal of Geophysical Research: Atmospheres, 99, 8183–8195, 1994.

Liu, Y., Liu, C. X., Wang, H. P., Tie, X. X., Gao, S. T., Kinnison, D., and Brasseur, G.: Atmospheric tracers during the 2003–2004 stratospheric warming event and impact of ozone intrusions in the troposphere, Atmospheric Chemistry and Physics, 9, 2157–2170, https://doi.org/10.5194/acp-9-2157-2009, 2009.

Flemming, J., Inness, A., Jones, L., Eskes, H. J., Huijnen, V., Schultz, M. G., Stein, O., Cariolle, D., Kinnison, D., and Brasseur, G.: Forecasts and assimilation experiments of the Antarctic ozone hole 2008, Atmospheric Chemistry and Physics, 11, 1961–1977, https://doi.org/10.5194/acp-11-1961-2011, 2011.

Søvde, O. A., Matthes, S., Skowron, A., Iachetti, D., Lim, L., Owen, B., Hodnebrog, Ø., Di Genova, G., Pitari, G., Lee, D. S., Myhre, G., and Isaksen, I. S. A.: Aircraft emission mitigation by changing route altitude: A multi-model estimate of aircraft NOx emission impact on O3 photochemistry, Atmospheric Environment, 95, 468–479, https://doi.org/10.1016/J.ATMOSENV.2014.06.049, 2014.

https://doi.org/10.5194/egusphere-2024-2866
Preprint. Discussion started: 30 September 2024

Skowron, A., Lee, D. S., and De León, R. R.: The assessment of the impact of aviation NOx on ozone and other radiative forcing responses – The importance of representing cruise altitudes accurately, Atmospheric Environment, 74, 159–168, https://doi.org/10.1016/J.ATMOSENV.2013.03.034, 2013.

Skowron, A., Lee, D. S., and De León, R. R.: Variation of radiative forcings and global warming potentials from regional aviation NO x emissions, Atmospheric Environment, 104, 69–78, https://doi.org/10.1016/j.atmosenv.2014.12.043, 2015.

Freeman, S., Lee, D. S., Lim, L. L., Skowron, A., and De León, R. R.: Trading off Aircraft Fuel Burn and NOx Emissions for Optimal Climate Policy, Environ. Sci. Technol., 52, 2498–2505, https://doi.org/10.1021/acs.est.7b05719, 2018.

Sander, S. P., Finlayson-Pitts, B., Friedl, R. R., Golden, D. M., Huie, R., Keller-Rudek, H., Kolb, C. E., Kurylo, M., Molina, M., Moortgat, G., Orkin, V., Ravishankara, A. R., and Wine, P.: Chemical Kinetics and Photochemical Data for Use in Atmospheric Studies, Evaluation No. 15, 2006.

Meinshausen, M., Nicholls, Z. R. J., Lewis, J., Gidden, M. J., Vogel, E., Freund, M., Beyerle, U., Gessner, C., Nauels, A., Bauer, N., Canadell, J. G., Daniel, J. S., John, A., Krummel, P. B., Luderer, G., Meinshausen, N., Montzka, S. A., Rayner, P. J., Reimann, S., Smith, S. J., van den Berg, M., Velders, G. J. M., Vollmer, M. K., and Wang, R. H. J.: The shared socio-economic pathway (SSP) greenhouse gas concentrations and their extensions to 2500, Geosci. Model Dev., 13, 3571–3605, https://doi.org/10.5194/gmd-13-3571-2020, 2020.

Houweling, S., Dentener, F., and Lelieveld, J.: The impact of nonmethane hydrocarbon compounds on tropospheric photochemistry, Journal of Geophysical Research: Atmospheres, 103, 10673–10696, https://doi.org/10.1029/97JD03582, 1998.

Zhang, J., Wuebbles, D., Pfaender, J. H., Kinnison, D., and Davis, N.: Potential Impacts on Ozone and Climate From a Proposed Fleet of Supersonic Aircraft, Earth's Future, 11, e2022EF003409, https://doi.org/10.1029/2022EF003409, 2023.

Kinnison, D., Brasseur, G. P., Baughcum, S. L., Zhang, J., and Wuebbles, D.: The Impact on the Ozone Layer of a Potential Fleet of Civil Hypersonic Aircraft, Earth's Future, 8, https://doi.org/10.1029/2020ef001626, 2020.

Strahan, S. E. and Polansky, B. C.: Meteorological implementation issues in chemistry and transport models, Atmospheric Chemistry and Physics, 6, 2895–2910, https://doi.org/10.5194/acp-6-2895-2006, 2006.

Revell, L. E., Tummon, F., Stenke, A., Sukhodolov, T., Coulon, A., Rozanov, E., Garny, H., Grewe, V., and Peter, T.: Drivers of the tropospheric ozone budget throughout the 21st century under the medium-high climate scenario RCP 6.0, Atmospheric Chemistry and Physics, 15, 5887–5902, https://doi.org/10.5194/acp-15-5887-2015, 2015.

Roeckner, E., Brokopf, R., Esch, M., Giorgetta, M., Hagemann, S., Kornblueh, L., Manzini, E., Schlese, U., and Schulzweida, U.: Sensitivity of Simulated Climate to Horizontal and Vertical Resolution in the ECHAM5 Atmosphere Model, Journal of Climate, 19, 3771–3791, https://doi.org/10.1175/JCLI3824.1, 2006.

Cohen, Y., Hauglustaine, D., Sauvage, B., Rohs, S., Konjari, P., Bundke, U., Petzold, A., Thouret, V., Zahn, A., and Ziereis, H.: Evaluation of modelled climatologies of O_3, CO, water vapour and NO$_{y}$ in the upper troposphere–lower stratosphere using regular in situ observations by passenger aircraft, Atmospheric Chemistry and Physics, 23, 14973, https://doi.org/10.5194/acp-23-14973-2023, 2023.

Rosenfield, J. E. and Douglass, A. R.: Doubled CO2 effects on NOy in a coupled 2D model, Geophysical Research Letters, 25, 4381–4384, https://doi.org/10.1029/1998GL900147, 1998.

van 't Hoff, J.A., Hauglustaine, D., Pletzer, J., Skowron, A., Grewe, V., Matthes, S., Meuser, M.M., Thor, R. N., Dedoussi, I.C.: Supporting dataset for "Intermodel comparison of the atmospheric composition changes due to emissions from a potential future supersonic aircraft fleet", Dataset, https://doi.org/10.4121/dd38833d-6c5d-47d8-bb10-7535ce1eecf1 (reserved DOI, to be minted on acceptance), 2024b

https://doi.org/10.5194/egusphere-2024-2866
Preprint. Discussion started: 30 September 2024

Appendices

Table A1: Summary of H_2O perturbations in all scenarios. Values calculated as triannual averages

	Strat. background H_2O[Tg]	Strat. H_2O perturbation [Tg]	Perturbation lifetime [month]	Hemispheric fraction [NH/SH]	Absolute Hemispheric fraction [NH/SH]
A1					
EMAC	4295.1	+69.34 (+1.62 %)	17.8	4.82	3.11
GEOS-Chem	7344.8	+49.34 (+0.67 %)	12.7	3.96	3.98
LMDZ-INCA	3743.8	+20.14 (+0.58 %)	5.2	5.37	5.37
MOZART-3	7520.6	+116.53 (+1.55 %)	30.0	4.56	4.48
Mean		+61.34 (+1.11 %)	16.4	4.68	4.24
A2					
EMAC	4295.1	+66.27 (+1.54 %)	17.0	7.05	3.17
GEOS-Chem	7344.8	+49.79 (+0.68 %)	12.8	3.88	3.89
LMDZ-INCA	3743.8	+20.55 (+0.55 %)	5.3	5.11	5.10
Mean		+45.54 (+0.92 %)	7.48	5.35	4.05
A3					
EMAC	4295.1	+19.69 (+0.46 %)	11.2	-25.07	2.39
GEOS-Chem	7344.8	+5.96 (+0.08 %)	3.4	10.19	10.39
LMDZ-INCA	3743.8	+2.37 (+0.06%)	1.3	36.26	39.41
Mean		+9.34 (+0.20 %)	5.3	8.89	17.40

https://doi.org/10.5194/egusphere-2024-2866
Preprint. Discussion started: 30 September 2024

Table A2: Summary of NO_x perturbations due to the emission scenarios. Values calculated as triannual averages.

	Strat background NO_x [Gg NO_2]	Strat NO_x perturbation [Gg NO2]	Perturbation lifetime [months]	Hemispheric fraction [NH/SH]	Absolute hemispheric fraction [NH/SH]
A1					
EMAC	2321.7	+38.71 (+1.67%)	4.2	5.29	2.41
GEOS-Chem	2302.0	+43.52 (+1.89%)	4.7	2.66	2.63
LMDZ-INCA	2457.8	+42.56 (+1.73%)	4.6	2.24	2.27
MOZART-3	1233.14	+39.07 (+3.16 %)	4.2	2.94	2.95
Mean		+40.96 (+2.11 %)	4.4	3.28	2.57
A2					
EMAC	2321.7	+139.6 (+6.01 %)	3.3	3.70	3.06
GEOS-Chem	2302.0	+173.6 (+7.54 %)	4.1	2.47	2.48
LMDZ-INCA	2457.8	+119.54 (+4.86 %)	2.8	2.30	2.31
MOZART-3	1233.14	+120.74 (+9.79 %)	2.8	3.09	3.08
Mean		+138.37 (+7.05 %)	3.3	2.89	2.73
A3					
EMAC	2321.7	+21.32 (+0.92 %)	5.4	5.58	1.96
GEOS-Chem	2302.0	+23.72 (+1.03 %)	6.0	2.60	2.67
LMDZ-INCA	2457.8	+17.41 (+0.71 %)	4.4	2.2	2.31
Mean		+20.82 (+0.89 %)	5.3	3.5	2.3

https://doi.org/10.5194/egusphere-2024-2866
Preprint. Discussion started: 30 September 2024

Table A3: Summary of O_3 perturbations due to the emission scenarios. Values calculated as triannual averages.

	Strat. background O3 [Tg]	Strat. O_3 perturbation [Tg]	Background column [DU]	Column perturbation [DU]	Absolute hemispheric mass fraction [NH/SH]
A1					
EMAC	3152.8	-1.13 (-0.04 %)	342.9	+0.09 (+0.03 %)	1.45
GEOS-Chem	3002.9	-5.88 (-0.20 %)	333.12	-0.72 (-0.22 %)	1.87
LMDZ-INCA	3092.0	-1.84 (-0.06 %)	337.6	-0.15 (-0.05 %)	1.57
MOZART-3	1907.4	-2.39 (-0.13 %)	238	-0.43 (-0.18%)	1.68
Mean		-2.81 (-0.11 %)	312.9	-0.30 (-0.11 %)	1.64
A2					
EMAC	3152.8	-8.19 (-0.26 %)	342.9	-0.611 (-0.18 %)	1.77
GEOS-Chem	3002.9	-14.06 (-0.46 %)	333.12	-1.36 (-0.41%)	1.61
LMDZ-INCA	3092.0	-4.72 (-0.15 %)	337.6	-0.30 (-0.09 %)	1.55
MOZART-3	1907.4	-9.17 (-0.48 %)	238	-1.35 (-0.57 %)	1.95
Mean		-9.04 (-0.34 %)	312.9	-0.91 (-0.31 %)	1.72
A3					
EMAC	3152.8	+0.21 (+0.01 %)	342.9	+0.11 (+0.03 %)	1.51
GEOS-Chem	3002.9	-0.63 (-0.02 %)	333.12	-0.04 (-0.01 %)	1.63
LMDZ-INCA	3092.0	+0.827 (+0.03 %)	337.6	+0.14 (+0.04 %)	1.43
Mean		+0.556 (+0.02 %)	337.9	+0.07 (+0.02 %)	1.52

https://doi.org/10.5194/egusphere-2024-2866
Preprint. Discussion started: 30 September 2024

Table A4: Summary of background halogen mixing ratios for the baseline (A0) scenario. Units in pptv. Values denoted by – indicate species which are not present in that specific model.

	Surface				200 to 10 hPa			
	EMAC	GEOS-Chem	LMDZ-INCA	MOZART-3	EMAC	GEOS-Chem	LMDZ-INCA	MOZART3
Br	0.0002	0.0002	0.0001	3.0153e-5	0.1730	0.1252	0.1026	0.1709
BrCl	1.9678e-6	0.0015	5.652e-7	4.5890e-7	0.5050	1.3526	0.3435	0.4528
BrO	0.0060	0.0028	0.0020	0.0006	2.7007	1.8154	1.3145	2.6226
CFC11	-	138.19	138.1999	248.0824	-	59.7229	70.9768	120.1767
Cl	1.8753e-6	2.0481	2.5670	3.3410	0.0189	0.02414	0.0213	0.0262
Cl_2	4.9708e-6	0.0028	1.9384	2.6432	7.5453	5.6160	4.3763	2.0720
Cl_2O_2	1.7003e-11	1.243e-9	7.8370	2.1778	4.4737	18.0780	8.6143	13.3571
$ClNO_2$	3.2010e-8	0.0706	0.0005	-	0.0303	0.0050	0.1487	-
$ClONO_2$	0.02210	0.0106	0.2481	0.2723	201.1863	265.0219	197.7726	309.8003
HBr	0.1244	0.01407	0.1085	0.0131	0.4284	0.1884	0.1691	0.2867
HCl	1.4150	3.2963	2.5572	1.6588	669.4262	680.3545	561.8869	936.3695
HOBr	0.0806	0.0116	0.0113	0.0032	1.0023	0.8293	1.1495	1.1218
HOCl	0.1142	0.0973	0.0587	0.0626	9.3144	20.2350	10.6867	8.4008
OClO	4.5830e-5	7.906e-5	0.2534	4.2968e-7	1.7333	1.9323	1.8834	2.1081

https://doi.org/10.5194/egusphere-2024-2866
Preprint. Discussion started: 30 September 2024

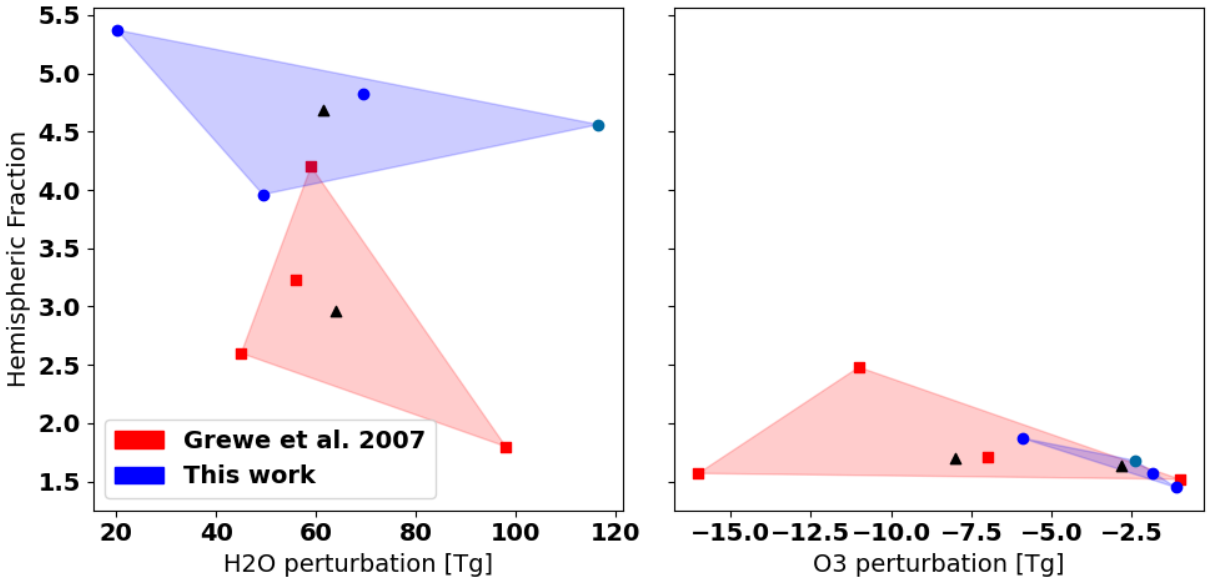

Fig A1: Comparison of the H2O (left) and O3 (right) perturbations and hemispheric fractions for the models used in this work and Grewe et al. (2007). Black triangles represent the multi-model means.

https://doi.org/10.5194/egusphere-2024-2866
Preprint. Discussion started: 30 September 2024

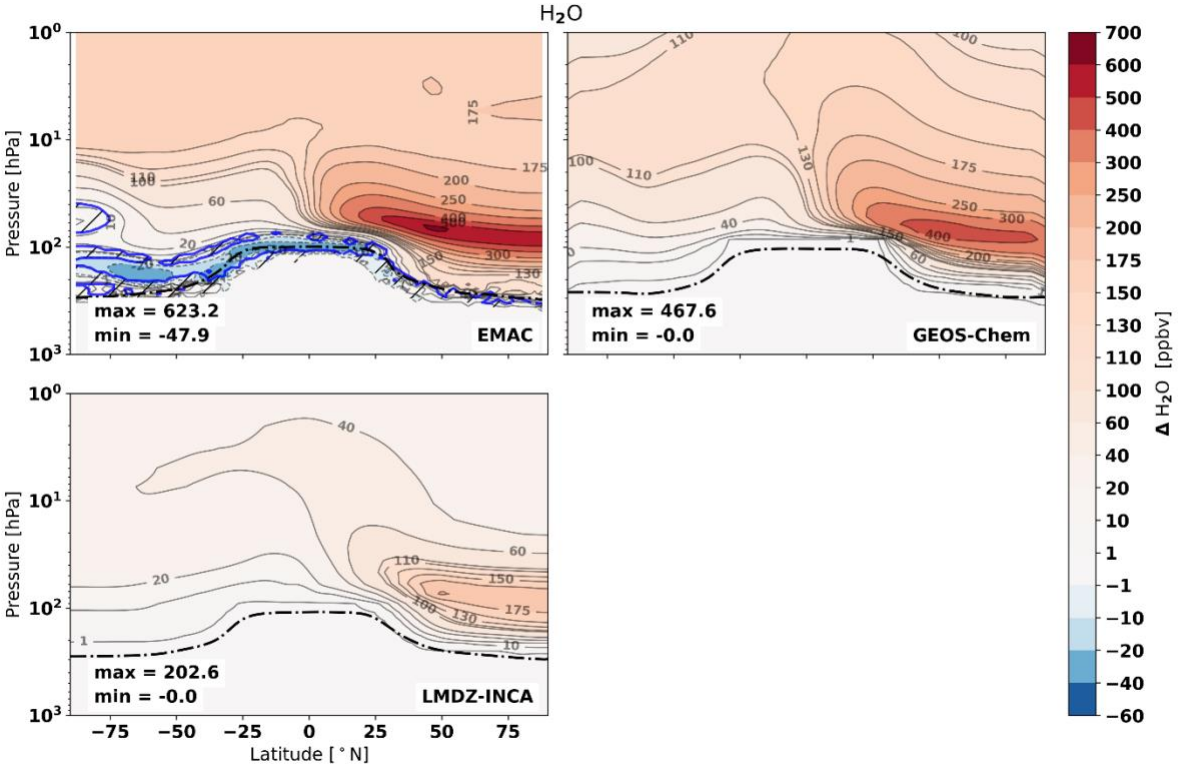

Fig A2: Changes in H2O volume mixing ratios for the triple NO_x (A2) emission scenario. Hatched areas enclosed by blue lines indicate regions which are not statistically significant for the EMAC results.

https://doi.org/10.5194/egusphere-2024-2866
Preprint. Discussion started: 30 September 2024

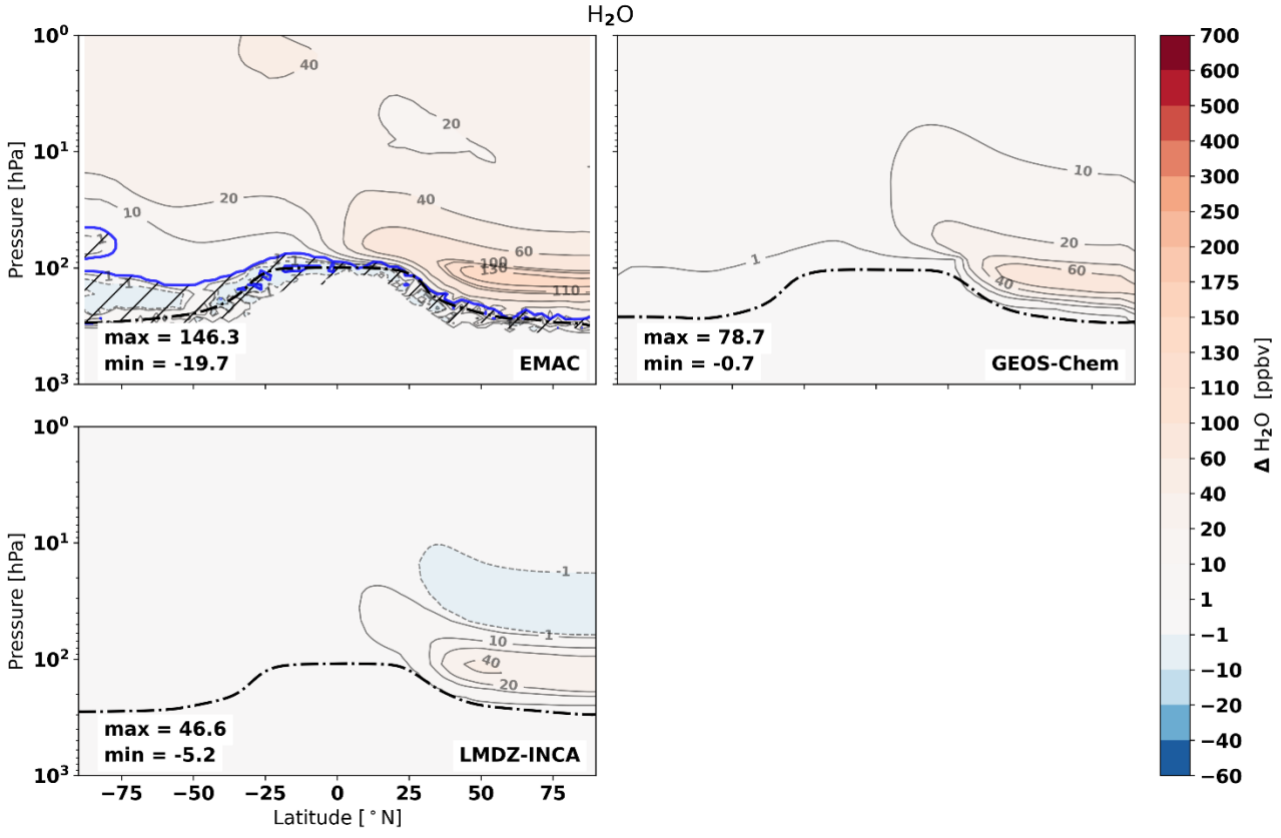

Fig A3: Changes in H2O volume mixing ratios for the low cruise (A3) emission scenario. Hatched areas enclosed by blue lines indicate regions which are not statistically significant for the EMAC results.

850

https://doi.org/10.5194/egusphere-2024-2866
Preprint. Discussion started: 30 September 2024

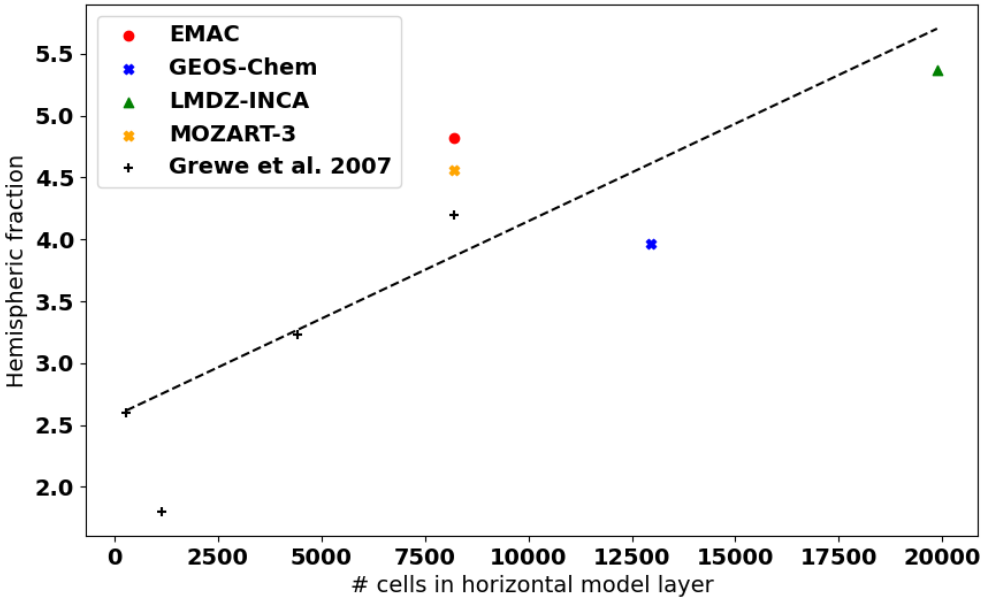

Fig A4: Hemispheric fraction of the water vapour perturbation (perturbation mass northern hemisphere / southern hemisphere) for the nominal supersonic emission scenario, over the number of cells in horizontal layers of the models used. The dashed line is a fitted first-order trend line.

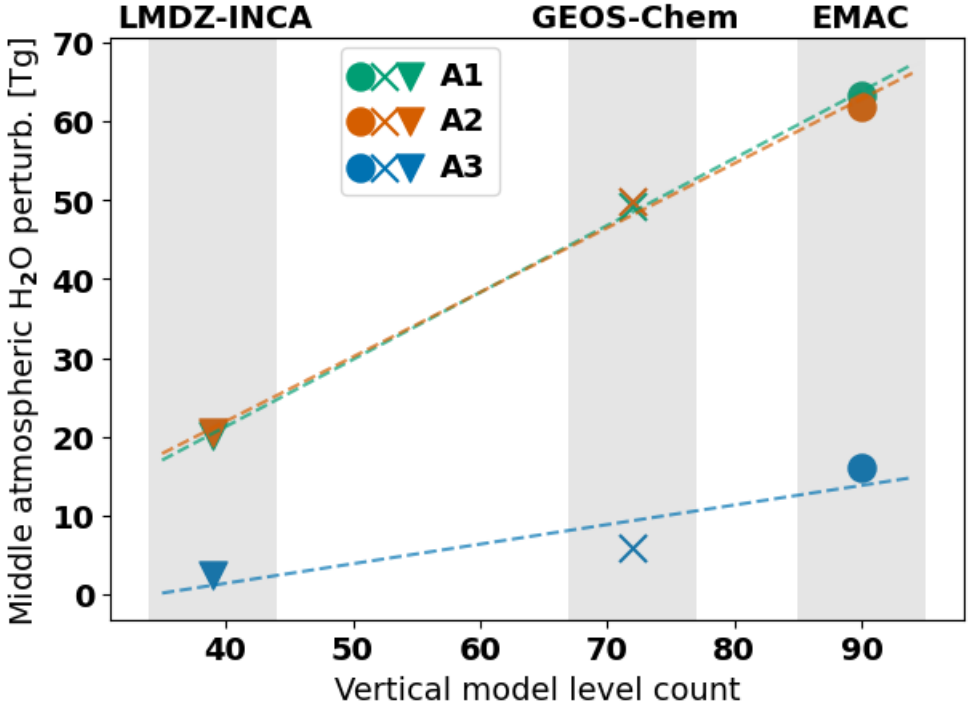

Fig A5: Stratospheric H_2O perturbation over the vertical model level count for the LMDZ-INCA, GEOS-Chem, and EMAC models for the emission scenarios.

https://doi.org/10.5194/egusphere-2024-2866
Preprint. Discussion started: 30 September 2024

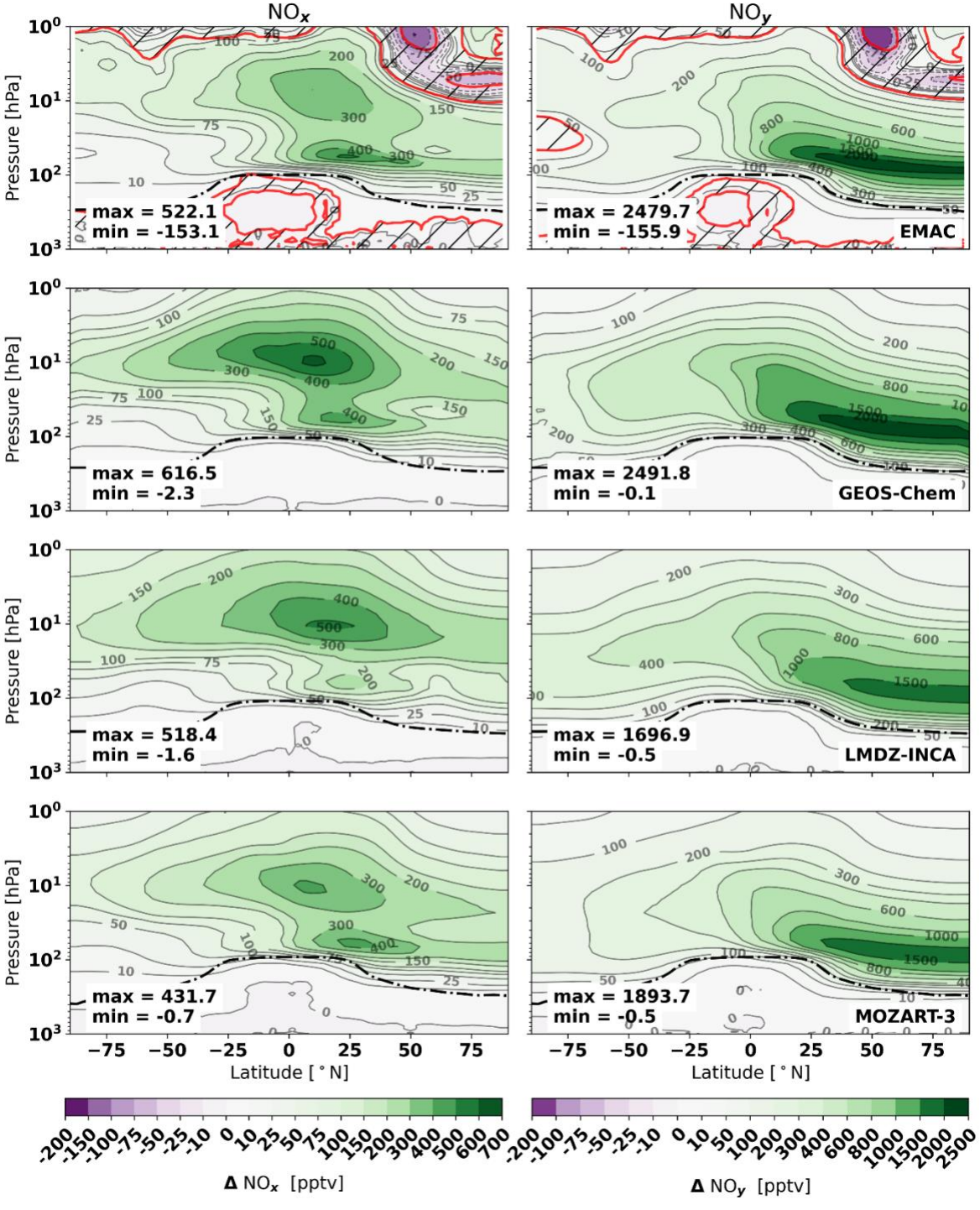

Fig A6: Mean changes in NO_x (left) and NO_y (right) concentrations in the triple NO_x (A2) emissions scenario across the models. Hatched areas enclosed by red lines indicate regions which are not statistically significant for the EMAC results.

https://doi.org/10.5194/egusphere-2024-2866
Preprint. Discussion started: 30 September 2024

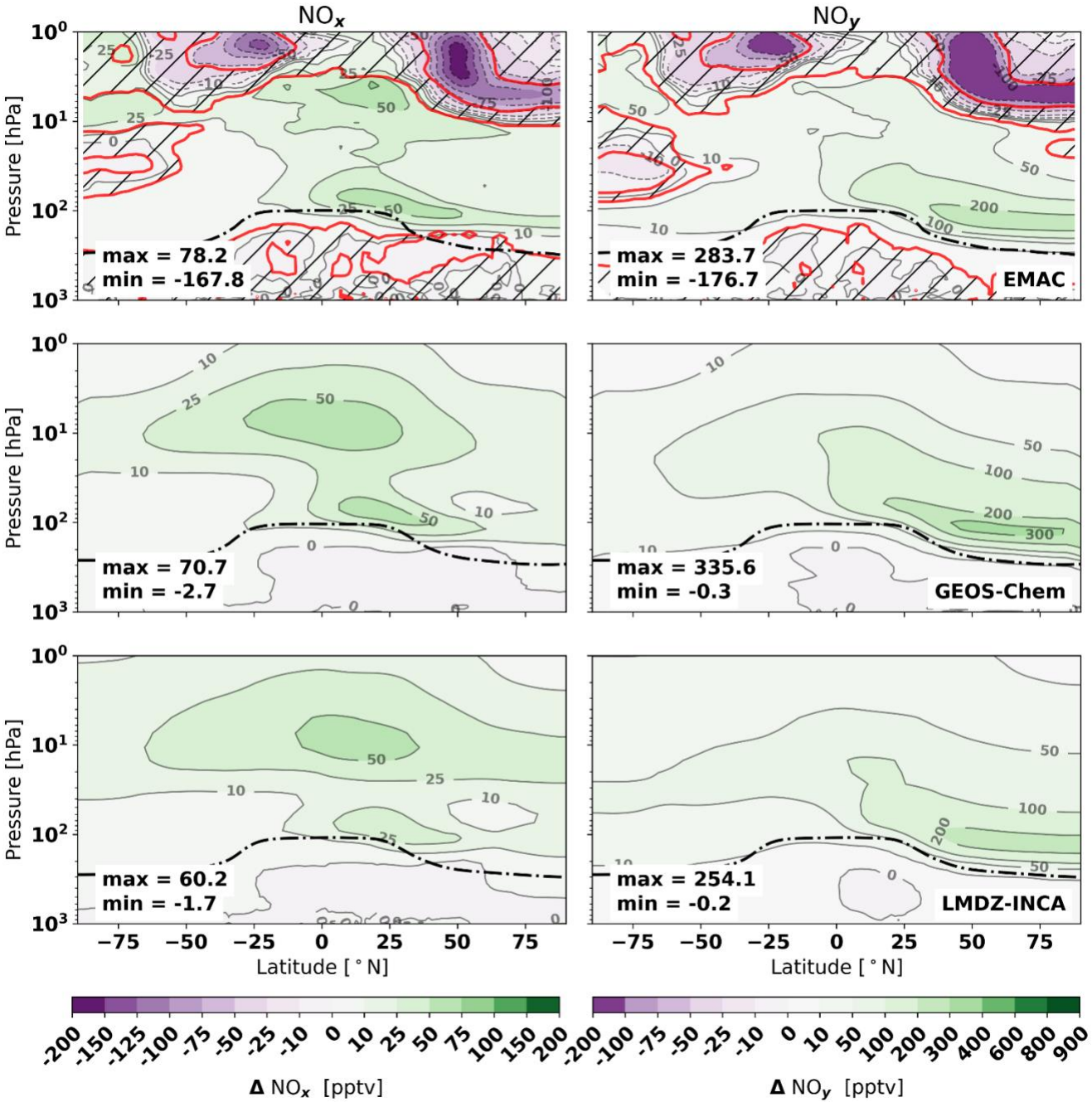

Fig A7: Similar to Fig Ax, but for the low cruise (A3) scenario. Hatched areas enclosed by red lines indicate regions which are not statistically significant for the EMAC results.

https://doi.org/10.5194/egusphere-2024-2866
Preprint. Discussion started: 30 September 2024

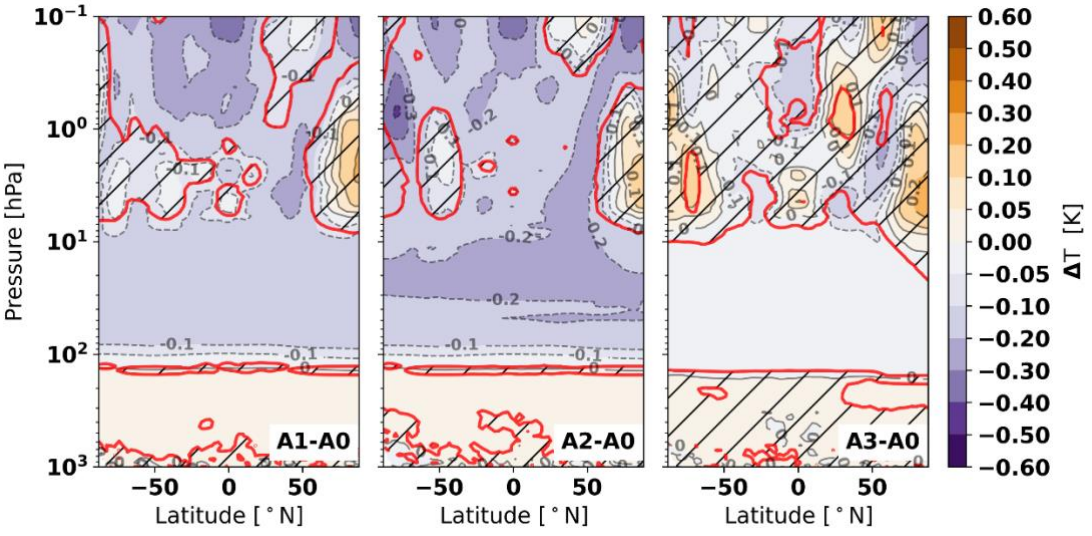

Fig A8: Average change in atmospheric temperature in Kelvin induced by the emission scenarios over the last 3 years of integration in the EMAC model. Hatched areas indicate areas where the change is not statistically significant.

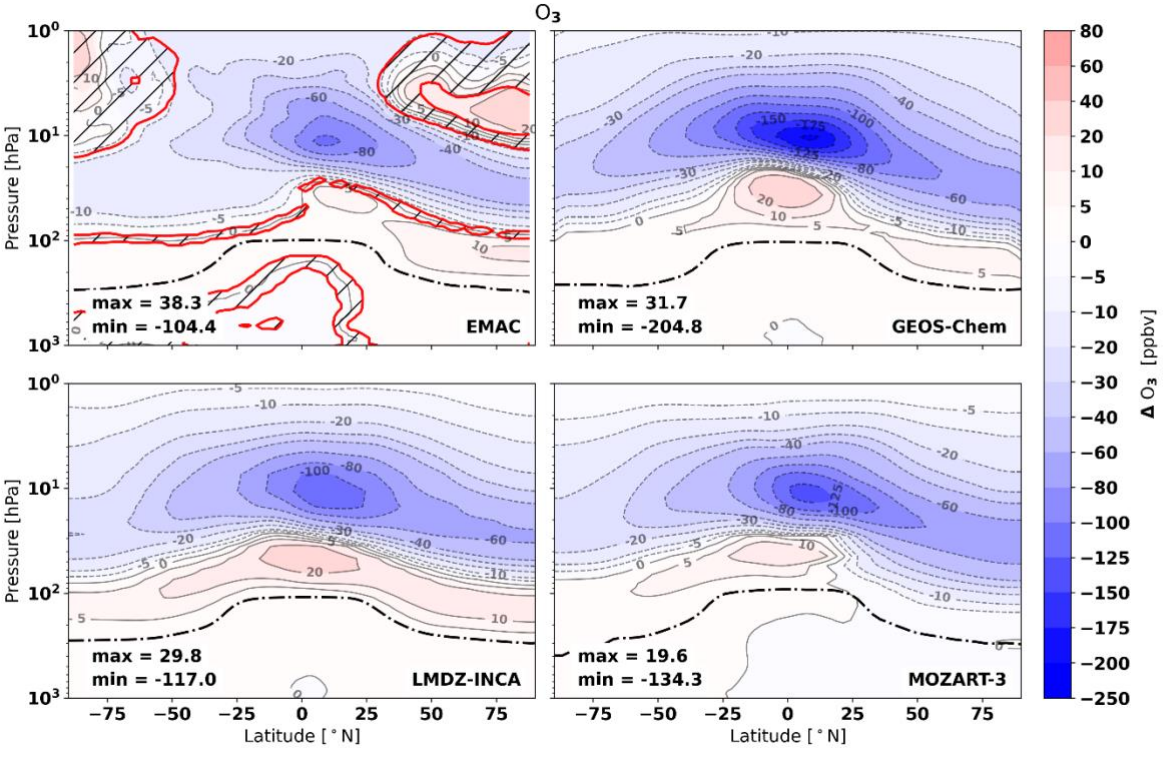

Fig A9: Changes in ozone VMR for the triple NO_x (A2) emissions scenario. Hatched areas enclosed by red lines indicate regions which are not statistically significant for the EMAC results.

https://doi.org/10.5194/egusphere-2024-2866
Preprint. Discussion started: 30 September 2024

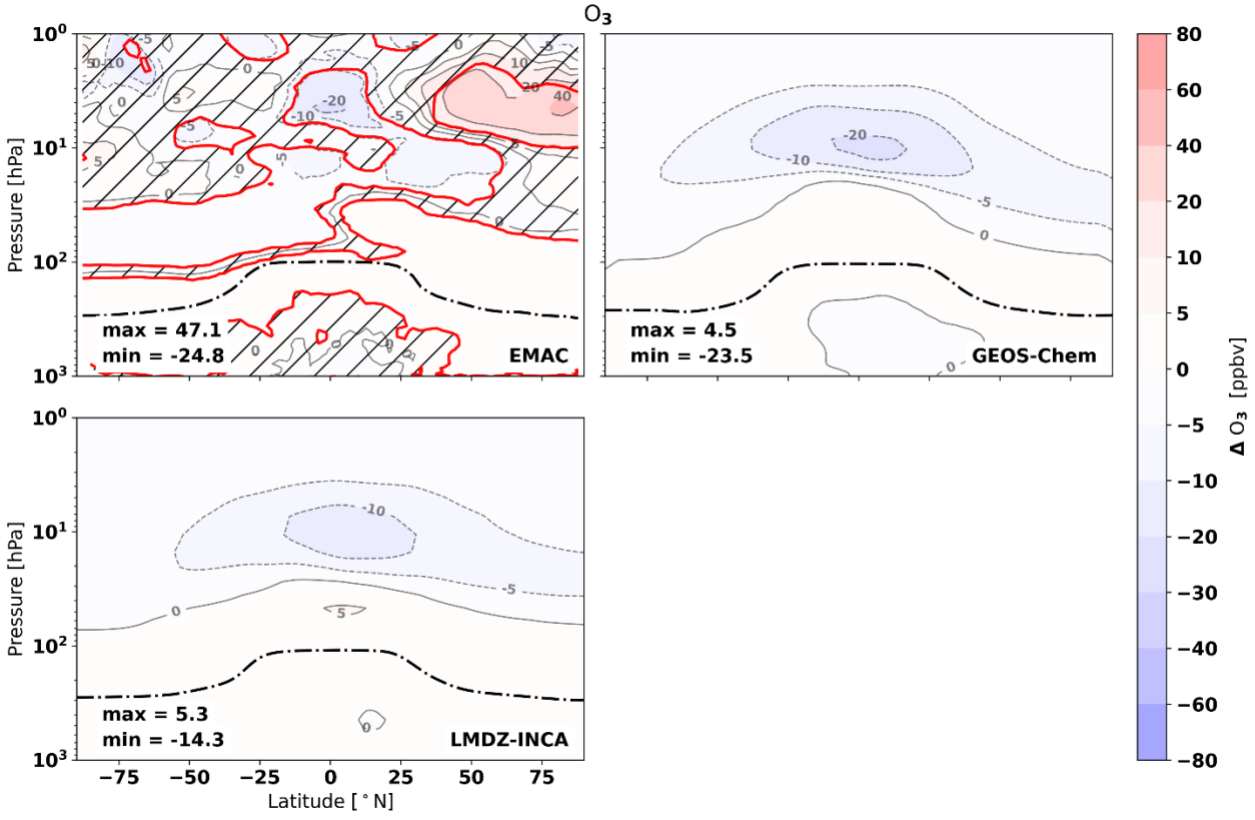

Fig A10: Similar to Fig. Ax, but for the low cruise (A3) scenario. Hatched areas enclosed by red lines indicate regions which are not statistically significant for the EMAC results.

https://doi.org/10.5194/egusphere-2024-2866
Preprint. Discussion started: 30 September 2024

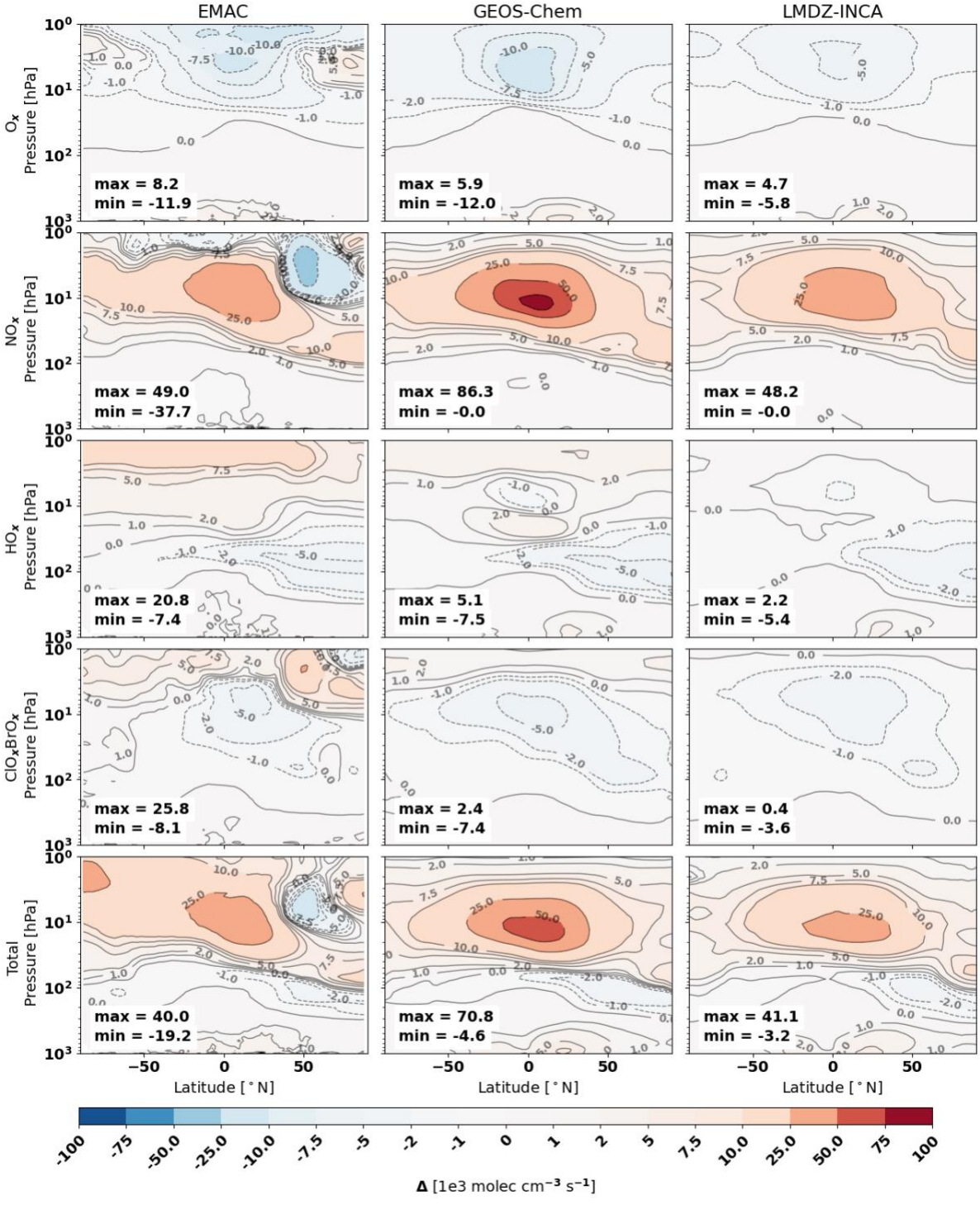

875 **Fig A11: Same as Fig 8 but for the triple NO_x (A2) emissions scenario**

https://doi.org/10.5194/egusphere-2024-2866
Preprint. Discussion started: 30 September 2024

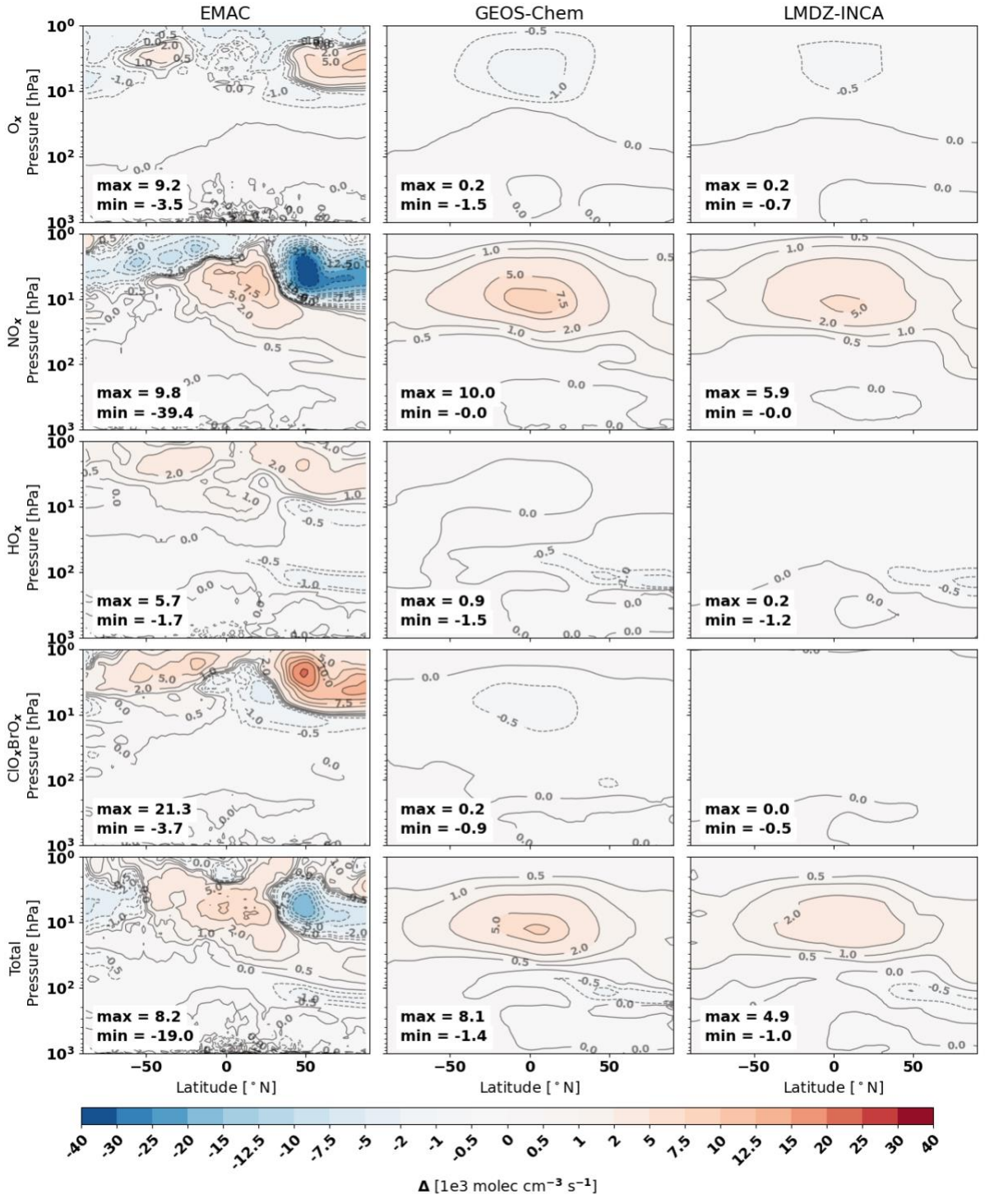

Fig A12: Same as Fig 8 but for the low cruise (A3) emissions scenario

https://doi.org/10.5194/egusphere-2024-2866
Preprint. Discussion started: 30 September 2024

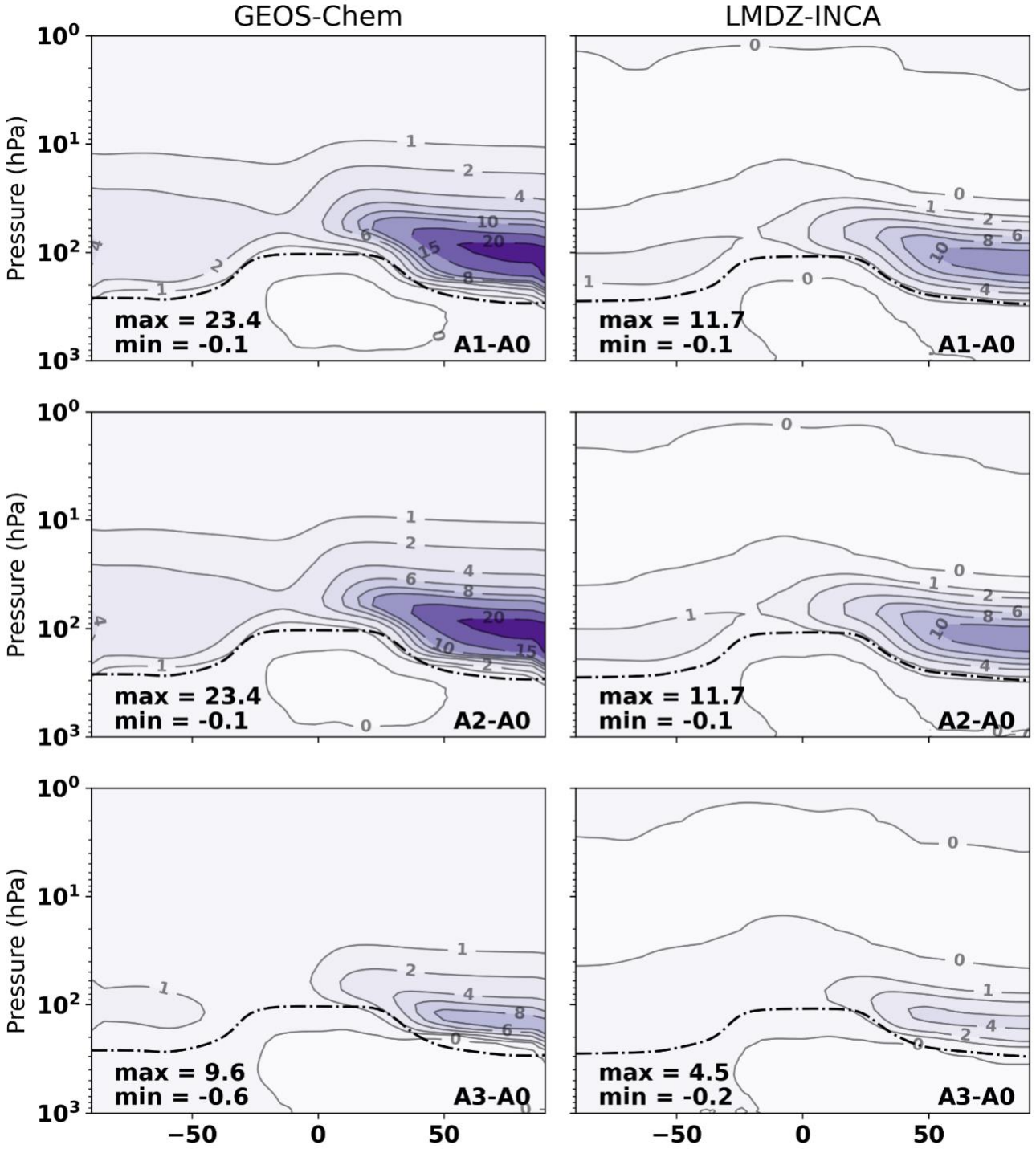

Fig A13: Comparison of the black carbon aerosol perturbations in 10^{-2} ng / m^3 for the GEOS-Chem (left) and LMDZ-INCA (right) models.

https://doi.org/10.5194/egusphere-2024-2866
Preprint. Discussion started: 30 September 2024

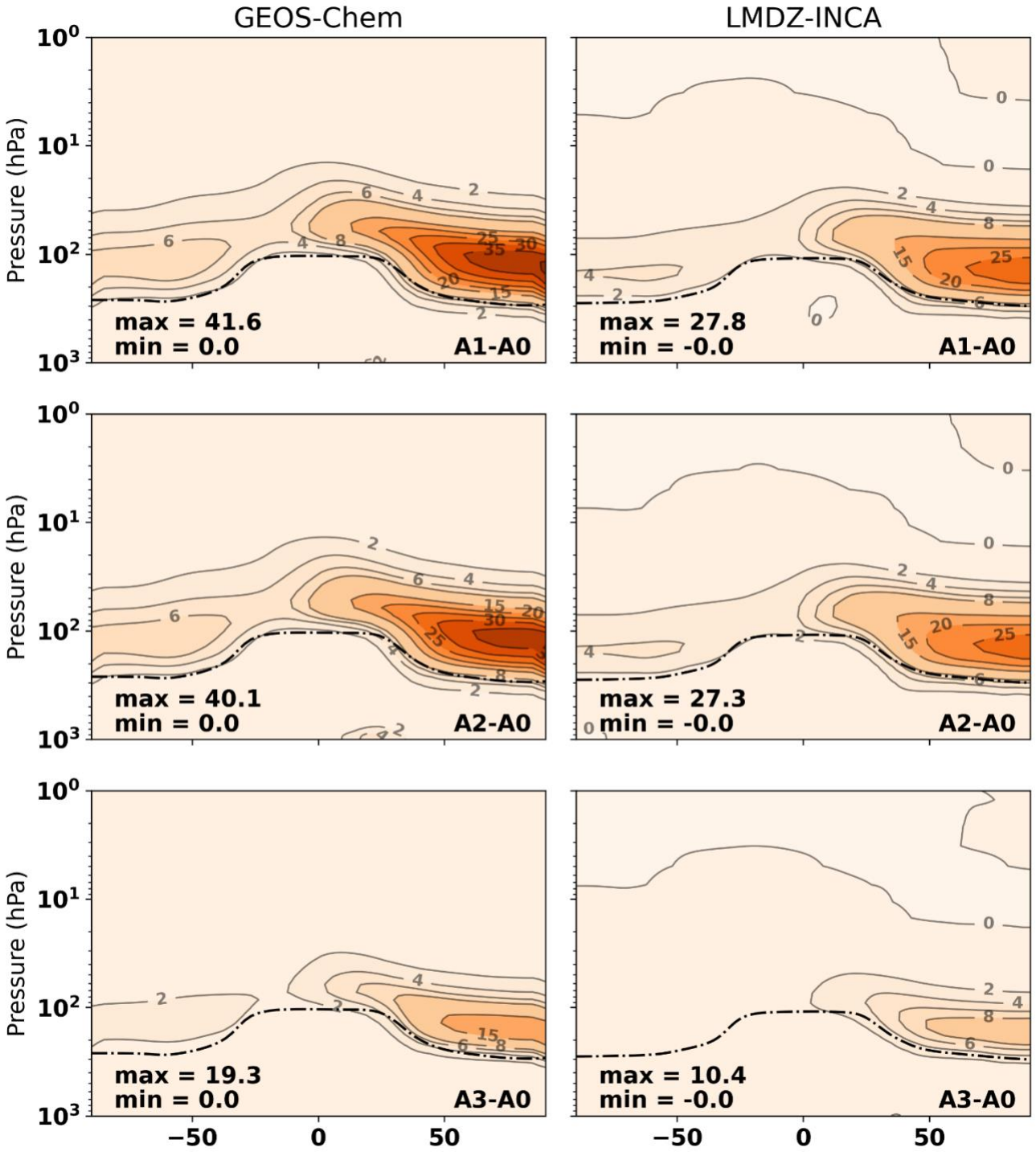

Fig A14: Comparison of the SO_4 aerosol perturbations in ng / m^3 for the GEOS-Chem (left) and LMDZ-INCA (right) models.